

1 Anoxia decreases the magnitude of the carbon, nitrogen, and phosphorus sink in freshwaters

2

3 Cayelan C. Carey^{1*}, Paul C. Hanson², R. Quinn Thomas^{1,3}, Alexandra B. Gerling¹, Alexandria

4 G. Hounshell¹, Abigail S. L. Lewis¹, Mary E. Lofton¹, Ryan P. McClure¹, Heather L. Wander¹,

5 Whitney M. Woelmer¹, B. R. Niederlehner¹, Madeline E. Schreiber⁴

6

7 ¹Department of Biological Sciences, Virginia Tech, Blacksburg, Virginia, USA 24061.

8 ²Center for Limnology, University of Wisconsin-Madison, Madison, Wisconsin, USA 53706.

9 ³Department of Forest Resources and Environmental Conservation, Virginia Tech, Blacksburg,
10 Virginia, USA 24061.

11 ⁴Department of Geosciences, Virginia Tech, Blacksburg, Virginia, USA 24061.

12 *Corresponding author. Email: cayelan@vt.edu; Phone: +1-540-231-8938

13

14 Submitted as a Primary Research Article to *Global Change Biology*

15

16 **Running head:** Anoxia disrupts freshwater C, N, and P cycles

17 **Author contributions:** Conceptualization: CCC, PCH, MES; Data curation: CCC, ABG, AGH,

18 ASL, MEL, RPM, HLW, WMW, BRN; Formal analysis: CCC, PCH, RQT; Investigation: CCC,

19 ABG, AGH, ASL, MEL, RPM, HLW, WMW, BRN, MES; Methodology: CCC, PCH, RQT;

20 Project administration: CCC; Software: RQT; Visualization: CCC, ASL, RPM, WMW, AGH,

21 HLW; Supervision: CCC, MES; Writing-original draft: CCC, MEL, BRN, AGH; Writing-review

22 & editing: CCC, PCH, RQT, ABG, AGH, ASL, MEL, RPM, HLW, WMW, BRN, MES

23 **Competing interests:** Authors declare that they have no competing interests.

24 **Data and materials availability:** All data and code are available in the Environmental Data
25 Initiative repository (Carey et al. 2019, Carey et al. 2020, Carey et al. 2021a, Carey et al. 2021b,
26 Carey et al. 2021e, Carey et al. 2021f) and Zenodo (Carey et al. 2021d).

28 **Abstract**

29 Oxygen availability is decreasing in many lakes and reservoirs worldwide, raising the urgency
30 for understanding how anoxia (low oxygen) affects coupled biogeochemical cycling, which has
31 major implications for water quality, food webs, and ecosystem functioning. Although the
32 increasing magnitude and prevalence of anoxia has been documented in freshwaters globally, the
33 challenges of disentangling oxygen and temperature responses have hindered assessment of
34 the effects of anoxia on carbon, nitrogen, and phosphorus concentrations, stoichiometry
35 (chemical ratios), and retention in freshwaters. The consequences of anoxia are likely severe and
36 may be irreversible, necessitating ecosystem-scale experimental investigation of decreasing
37 freshwater oxygen availability. To address this gap, we devised and conducted REDOX (the
38 Reservoir Ecosystem Dynamic Oxygenation eXperiment), an unprecedented, seven-year
39 experiment in which we manipulated and modeled bottom-water (hypolimnetic) oxygen
40 availability at the whole-ecosystem scale in a eutrophic reservoir. Seven years of data reveal that
41 anoxia significantly increased hypolimnetic carbon, nitrogen, and phosphorus concentrations and
42 altered elemental stoichiometry by factors of 2-5 \times relative to oxic periods. Importantly,
43 prolonged summer anoxia increased nitrogen export from the reservoir by six-fold and changed
44 the reservoir from a net sink to a net source of phosphorus and organic carbon downstream.
45 While low oxygen in freshwaters is thought of as a response to land use and climate change,
46 results from REDOX demonstrate that low oxygen can also be a *driver* of major changes to

47 freshwater biogeochemical cycling, which may serve as an intensifying feedback that increases
48 anoxia in downstream waterbodies. Consequently, as climate and land use change continue to
49 increase the prevalence of anoxia in lakes and reservoirs globally, it is likely that anoxia will
50 have major effects on freshwater carbon, nitrogen, and phosphorus budgets as well as water
51 quality and ecosystem functioning.

52

53 **Keywords:** Biogeochemistry, Ecosystem modeling, Hypoxia, Nutrient retention, Oxygen,
54 REDOX, Reservoir, Stoichiometry, Water quality, Whole-ecosystem experiment

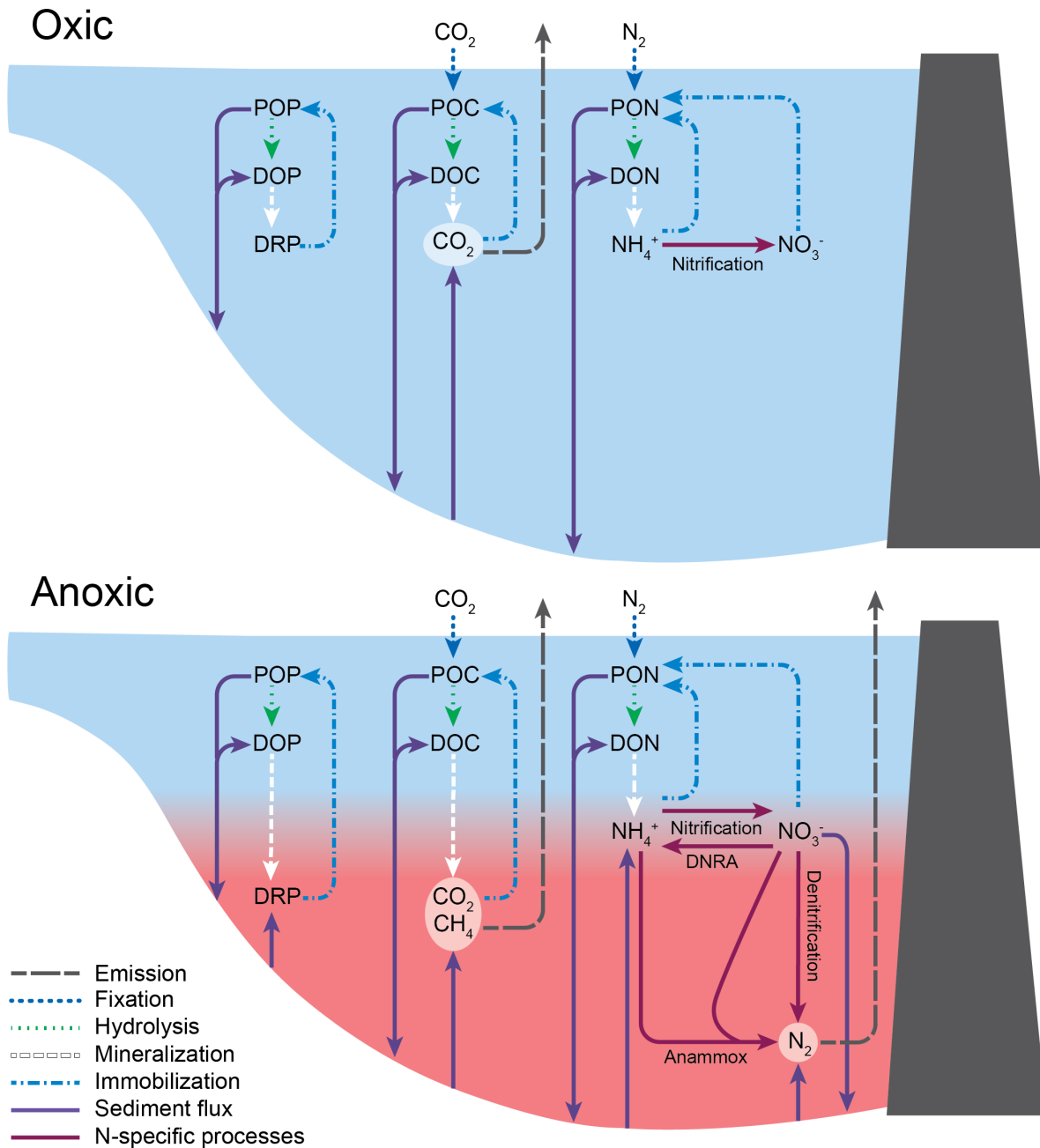
55

56 **Introduction**

57 Oxygen concentrations in lakes and reservoirs around the world are decreasing, which
58 has the potential to substantially alter freshwater ecosystem functioning and water quality. As a
59 result of climate and land use change, low oxygen availability (anoxia) is becoming more
60 common in the hypolimnion, or bottom waters, of many lakes and reservoirs (Jenny et al. 2016a,
61 Jane et al. 2021, Woolway et al. 2021). An increase in both the occurrence and duration of
62 hypolimnetic anoxia in freshwaters is likely to substantially alter the cycles of carbon (C),
63 nitrogen (N), and phosphorus (P), three fundamental elements that determine freshwater food
64 web structure, water quality, and ecosystem functioning (Sterner and Elser 2002, Kortelainen et
65 al. 2013). In particular, anoxia could disrupt the critical role of freshwater ecosystems as C, N,
66 and P sinks in global biogeochemical cycles. Freshwaters retain 72% of the organic C, 56% of
67 the total N, and 56% of the total P exported from land via sediment burial or release to the
68 atmosphere, preventing these elements from being transported to downstream freshwater
69 ecosystems or the oceans (Maranger et al. 2018). Altogether, the consequences of anoxia for C,

70 N, and P concentrations, stoichiometry (chemical ratios), and retention in freshwaters are likely
71 severe and may be irreversible (Nürnberg 1988, Søndergaard et al. 2003, Brothers et al. 2014,
72 North et al. 2014), necessitating ecosystem-scale investigation of how hypolimnetic anoxia
73 affects freshwaters.

74 Biogeochemical cycles of dissolved and total C, N, and P will likely respond differently
75 to hypolimnetic anoxia (Fig. 1). In the bottom waters of lakes and reservoirs, we expect
76 dissolved organic C (DOC) concentrations to be higher in anoxic than oxic conditions, as DOC is
77 mineralized much more efficiently by oxygen than by alternate terminal electron acceptors
78 (Walker and Snodgrass 1986, Beutel 2003). Moreover, anoxia has been shown to stimulate the
79 release of DOC from sediments to the water column (Fig. 1; Brothers et al. 2014, Peter et al.
80 2017), as well as increase hypolimnetic methane concentrations and subsequent greenhouse gas
81 emissions (Vachon et al. 2019, Hounshell et al. 2021). DOC generally dominates the total OC
82 (TOC) pool in lakes (Toming et al. 2020), thus we would expect TOC to exhibit similar
83 responses as DOC to anoxia. For hypolimnetic dissolved inorganic nitrogen (DIN), ammonium
84 (NH_4^+) concentrations would be expected to be higher in anoxic conditions due to
85 ammonification and release from sediments (Fig. 1; Rysgaard et al. 1994, Beutel et al. 2006). In
86 contrast, nitrate (NO_3^-) would be lower in anoxic than oxic conditions, as denitrification
87 decreases NO_3^- in the absence of oxygen while nitrification increases NO_3^- in the presence of
88 oxygen (Fig. 1; Sharma and Ahlert 1977, Downes 1987). Total nitrogen (TN) in the hypolimnion
89 could either increase or decrease in anoxic conditions, depending on the balance of NH_4^+ vs.
90 NO_3^- within the DIN pool, as the inorganic fraction of hypolimnetic dissolved N is generally
91 greater than the organic fraction (Kim et al. 2006). For hypolimnetic phosphorus (P), we would
92 expect that dissolved reactive phosphorus (DRP) concentrations would be higher in anoxic



93

94 **Fig. 1. Conceptual diagram of the dominant carbon, nitrogen, and phosphorus cycling**
 95 **processes (denoted by arrow lines) expected under oxic (top) and anoxic (bottom)**
 96 **conditions in the water column of a thermally stratified reservoir.** Carbon processes include
 97 cycling of carbon dioxide (CO₂), dissolved organic carbon (DOC), methane (CH₄), and
 98 particulate organic carbon (POC). Nitrogen processes include cycling of dissolved organic
 99 nitrogen (DON), nitrogen gas (N₂), ammonium (NH₄⁺), nitrate (NO₃⁻), and particulate organic
 100 nitrogen (PON). Phosphorus processes include cycling of dissolved organic phosphorus (DOP),
 101 dissolved reactive phosphorus (DRP), and particulate organic phosphorus (POP).

102 conditions as DRP is released into the water column during iron reduction and particulate
103 organic matter mineralization (Fig. 1; Mortimer 1971, Boström et al. 1988, Nürnberg 1988,
104 Rydin 2000). Total P (TP) concentrations would likely exhibit a similar but more muted response
105 to anoxia than DRP, as DRP is usually a small fraction of the TP pool (Wetzel 2001).

106 While these different C, N, and P processes have been well-studied individually, there
107 have been no studies on the net effect of anoxia on all of these cycles operating concurrently at
108 the ecosystem scale, likely due to the challenges of disentangling complex coupled
109 biogeochemical cycling with observational field studies or laboratory experiments. Explicitly
110 considering interconnected elemental cycles and their stoichiometry (following Sterner and Elser
111 2002) is essential to understanding the effects of anoxia on ecosystem functioning.

112 Increases in hypolimnetic anoxia have substantial implications for the fate of C, N, and P
113 in freshwater ecosystems. There are two primary fates for C, N, and P entering into a waterbody:
114 retention - by either remaining in the water column, burial in the sediments, or emission to the
115 atmosphere (for C and N only) - or export downstream (following the ecosystem retention
116 definition used by Dillon and Molot 1997, Harrison et al. 2009, Powers et al. 2015, Maranger et
117 al. 2018, and many others). Anoxia may decrease the ability of lakes and reservoirs to retain
118 NH_4^+ and DRP by reducing their burial in sediments (Rysgaard et al. 1994, North et al. 2014,
119 Powers et al. 2015), thereby increasing their downstream export. Conversely, anoxia could
120 increase the retention of NO_3^- by increasing its emission to the atmosphere via denitrification,
121 thereby decreasing its downstream export (Fig. 1; Beaulieu et al. 2014). For C, the ecosystem-
122 scale effects of anoxia are likely complex. The TOC pool includes dissolved and particulate
123 fractions of OC that may respond to oxygen differently and are mediated by ambient
124 environmental conditions, such as external loading, temperature, nutrients, and light (Hanson et

125 al. 2015). For example, anoxia could increase the retention of particulate OC (POC) by
126 decreasing its mineralization, thereby potentially increasing its burial in sediments (Walker and
127 Snodgrass 1986, Beutel 2003). Simultaneously, anoxia could decrease the retention of DOC by
128 stimulating fluxes of DOC from the sediments into the water column (e.g., by reductive
129 dissolution of iron-bound DOC complexes; Skoog and Arias-Esquivel 2009), thereby potentially
130 decreasing burial in sediments (Brothers et al. 2014, Peter et al. 2017), and increasing DOC
131 export downstream. Consequently, quantifying the effect of anoxia on C, N, and P retention vs.
132 downstream export (and thus determining if a waterbody is a sink or source of C, N, and P
133 downstream) is needed to improve our understanding of the changing role of lakes and reservoirs
134 in global biogeochemical cycles.

135 In particular, human-made reservoirs, which retain substantially more inflowing C, N,
136 and P per unit area than naturally formed lakes globally via either sediment burial or emissions to
137 the atmosphere (Harrison et al. 2009, Powers et al. 2016, Maranger et al. 2018), may be very
138 sensitive to the effects of hypolimnetic anoxia. Despite only covering 6-11% of the global lentic
139 surface (Downing et al. 2006, Lehner et al. 2011, Verpoorter et al. 2014), reservoirs alone are
140 estimated to account for ~40% of total annual global OC burial (Mendonça et al. 2017) and 26%
141 of total annual global P burial (Maranger et al. 2018). Moreover, reservoirs globally emit 6.5 Tg
142 N yr⁻¹ to the atmosphere, primarily via denitrification (Harrison et al. 2009, Beusen et al. 2016).
143 In an analysis of ~1000 lakes and reservoirs sampled once across the U.S., reservoirs were found
144 to have lower organic C:P and N:P ratios than naturally formed lakes, which was attributed in
145 part to a greater incidence of hypolimnetic anoxia in reservoirs than naturally formed lakes
146 (Maranger et al. 2018). However, that study lacked accompanying oxygen data to examine how
147 C, N, and P varied across a gradient of oxygen availability. Moreover, the amalgamation of data

148 from waterbodies with different climate and catchment land use makes it challenging to quantify
149 how changing oxygen alters water column C, N, and P concentrations, stoichiometry, and export.
150 We need new approaches that embrace the dynamic nature of reservoirs over time and allow us
151 to disentangle the effects of hypolimnetic anoxia on these waterbodies, especially as their
152 construction is increasing globally (Zarfl et al. 2015).

153 To mechanistically quantify the effects of anoxia on C, N, and P cycling, we devised and
154 conducted REDOX (the Reservoir Ecosystem Dynamic Oxygenation eXperiment), an
155 unprecedented, seven-year study that integrated a long-term hypolimnetic oxygenation
156 manipulation with ecosystem modeling in a eutrophic reservoir. Coupled whole-ecosystem
157 manipulations and ecosystem modeling provide a powerful approach for both quantifying the
158 effects of hypolimnetic anoxia on C, N, and P cycling and testing the mechanisms underlying
159 continental-scale patterns derived from thousands of waterbodies (e.g., Helton et al. 2015,
160 Maranger et al. 2018). Foundational work based on sediment core incubations in the laboratory
161 and small chambers placed *in situ* on the sediments of lakes and reservoirs (e.g., Frindte et al.
162 2015, Lau et al. 2016) have yet to be tested at the ecosystem scale, which is needed to overcome
163 the limitations of small volumes of water and mesocosm fouling. Studies that manipulate an
164 entire ecosystem are able to disentangle the effects of oxygen availability from other
165 environmental drivers, such as water temperature and biological activity, on C, N, and P cycling
166 (Cole 2013). However, it is logistically challenging to replicate these intensive experiments
167 under different meteorological and environmental conditions over time to assess robustness and
168 repeatability of ecosystem responses. Consequently, data from whole-ecosystem manipulations
169 can be used to calibrate ecosystem models (following Medlyn et al. 2015) that can simulate
170 complex ecosystem responses under a range of oxygen scenarios and weather conditions over

171 multiple years, thereby overcoming the constraints of separate empirical and model
172 investigations.

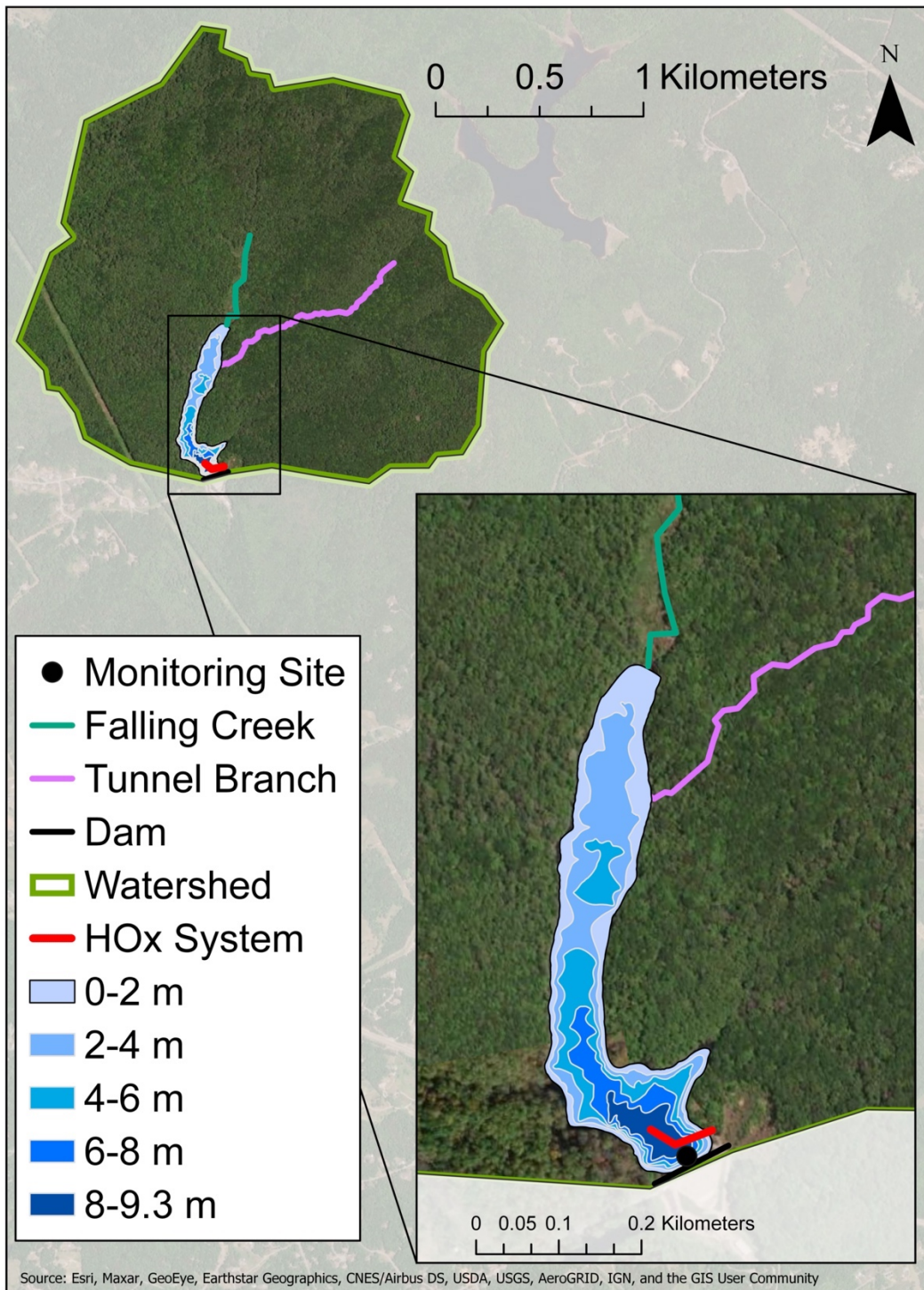
173 The purpose of REDOX was to study ecosystem-scale functioning under contrasting
174 oxygen conditions over multiple years in the same reservoir. First, we intensively monitored
175 dissolved oxygen and total and dissolved C, N, and P chemistry, as well as a suite of
176 accompanying water quality variables, in the reservoir during the seven-year field manipulation.
177 Second, we used the empirical data to calibrate a coupled hydrodynamic-ecosystem model,
178 which was used to quantify the effects of varying oxygen conditions over the seven years. To
179 investigate further changes in reservoir C, N, and P cycling due to anoxia, we used the calibrated
180 model to test hypolimnetic oxygen scenarios under a range of seasonal and meteorological
181 conditions. We focused on two contrasting model scenarios: one in which there was oxygenation
182 throughout the stratified summer periods in all seven years, resulting in continuous oxic
183 conditions, and one in which there was no oxygenation, resulting in hypolimnetic anoxia every
184 summer. We used the model output to address the following questions: 1) How does
185 hypolimnetic oxygen availability affect total and dissolved C, N, and P concentrations and
186 stoichiometry?, and 2) How does hypolimnetic anoxia affect reservoir retention and downstream
187 export of C, N, and P?

188

189 **Materials and Methods**

190 *Site description*

191 We studied the effect of changing oxygen conditions on C, N, and P dynamics in Falling
192 Creek Reservoir (FCR), a small eutrophic reservoir located in Vinton, Virginia, USA
193 (37.303479,-79.837371; Fig. 2). FCR has a maximum depth of 9.3 m and surface area of 0.119



194
 195 **Fig. 2. Map of Falling Creek Reservoir, Vinton, VA, USA (37.303479, -79.837371).** The map
 196 shows the reservoir watershed, locations of the two inflow streams (Falling Creek and Tunnel
 197 Branch), dam, hypolimnetic oxygenation (HOx) system, and monitoring site near the dam.

198 km² and is a drinking water source operated by the Western Virginia Water Authority (WVWA;
199 Gerling et al. 2014). FCR's watershed was farmland at the time of reservoir construction in 1898
200 and is almost completely deciduous forest today following agricultural abandonment in the
201 1930s (Gerling et al. 2016). The reservoir has never been dredged (Gerling et al. 2016), and had
202 a mean hydraulic residence time of 281 days (± 12 days, 1 S.E.) during our study. FCR has
203 hypolimnetic outtake valves from which water can be withdrawn for treatment.

204

205 *Whole-ecosystem manipulations*

206 We manipulated hypolimnetic oxygen availability in FCR using an engineered
207 hypolimnetic oxygenation system (HOx) deployed by the WVWA in 2012, which allowed us to
208 generate contrasting summer oxic and anoxic conditions (Gerling et al. 2014). The HOx system
209 withdraws hypolimnetic water from 8 m depth, injects dissolved oxygen into the water at super-
210 saturated concentrations onshore, and returns the oxygenated water back to the hypolimnion at 8
211 m without altering thermal stratification or water temperature (Gerling et al. 2014).

212 During the summers of 2013-2019, the HOx system was operated at variable oxygen
213 addition levels and durations in collaboration with the WVWA (Carey et al. 2021d). Some
214 summers experienced intermittent 4-week periods of oxygenation (2013, 2014); some summers
215 had near-continuous oxygenation (2015, 2016, 2017), one summer had approximately half
216 oxygenation (2018), and one summer experienced intermittent 2-week periods of oxygenation
217 (2019; Carey et al. 2021d). These wide-ranging oxygenation conditions, which occurred because
218 the reservoir was an actively managed drinking water source, provided an ideal dataset for
219 calibrating the biogeochemical rates in the ecosystem model to variable hypolimnetic oxygen
220 conditions, as described below.

221 *Monitoring data*

222 FCR's physics, chemistry, and biology were intensively monitored throughout the
223 REDOX manipulations (see Supplementary Text 1 for detailed sampling methods). On every
224 sampling day, depth profiles of water temperature and dissolved oxygen were collected at the
225 deepest site of the reservoir, near the dam (Carey et al. 2021b). We collected water samples for
226 total and dissolved N, P, and organic C (hereafter, C) analyses from the reservoir's water
227 treatment extraction depths (0.1, 1.6, 2.8, 3.8, 5.0, 6.2, 8.0, and 9.0 m) using a Van Dorn
228 sampler. Water was filtered through glass-fiber 0.7-micron filters into acid-washed bottles and
229 immediately frozen until analysis for dissolved C, N, and P samples (Carey et al. 2021e).
230 Unfiltered water was frozen in separate acid-washed bottles for total samples (Carey et al.
231 2021e). We focused our sampling and analysis on organic C, rather than inorganic C, because of
232 the important role of reservoirs in burying this pool in the global C cycle (Mendonça et al. 2017),
233 and because previous work indicates that most terrestrial dissolved inorganic C loads are rapidly
234 emitted to the atmosphere (McDonald et al. 2013).

235 We used standard methods for biogeochemical analyses (see Supplementary Text 2 for
236 detailed laboratory methods). We used flow injection analysis to determine concentrations of N
237 and P colorimetrically (APHA 2017), with an alkaline persulfate digestion for TN and TP
238 fractions. DOC and TOC were determined by either heated persulfate digestion or high-
239 temperature combustion followed by infrared absorbance (APHA 2017; see Table S1). All field
240 and laboratory data are available with metadata in the Environmental Data Initiative (EDI)
241 repository (Carey et al. 2019, Carey et al. 2020, Carey et al. 2021a, Carey et al. 2021b, Carey et
242 al. 2021e, Carey et al. 2021f).

243

244 *Model description and driver data*

245 We used the empirical data to calibrate and validate the General Lake Model coupled to
246 Aquatic EcoDynamics modules (GLM-AED, v.3.2.0a3) configured for FCR (see Supplementary
247 Text 3 for detailed modeling methods). GLM-AED is an open-source, 1-D numerical simulation
248 model that is widely used in the freshwater research community to model lakes and reservoirs
249 (e.g., Bruce et al. 2018, Hipsey et al. 2019, Farrell et al. 2020, Ward et al. 2020). GLM-AED
250 requires meteorological, inflow, and outflow driver data and simulates water balance and thermal
251 layers using a Lagrangian strategy (Hipsey et al. 2019). GLM-AED has a flexible structure in
252 which modules representing different ecosystem components can be turned on or off to recreate
253 varying levels of ecosystem complexity; our configuration for FCR included modules for
254 oxygen, C, silica (Si), N, P, organic matter, and phytoplankton (Carey et al. 2021c).

255 GLM-AED simulates the dominant processes controlling freshwater oxygen and C, N,
256 and P cycling (see Supplementary Text 3; Farrell et al. 2020, Ward et al. 2020). Biogeochemical
257 processes (e.g., sediment fluxes, mineralization) were modeled as a function of both oxygen
258 following Michaelis-Menten dynamics and temperature following Arrhenius coefficients (Farrell
259 et al. 2020). Consequently, processes that are favored in anoxic conditions (e.g., sediment fluxes
260 of DOC, NH_4^+ , and DRP into the hypolimnion) were still simulated in oxic conditions, but at
261 much lower rates.

262 The ecosystem model provided important insight on the effects of anoxia that would have
263 been impossible to obtain from the field manipulation alone. First, while we do report on the
264 biogeochemical responses to the field manipulation to provide complementary data to the model
265 output, ecosystems rarely experience such rapid shifting of redox conditions at sub-seasonal
266 scales, as were created by abrupt additions of oxygen via the HOx system. Thus, to understand

267 how our FCR results applied to other waterbodies, we used the seven-year field manipulation as
268 a proxy to contrast the consequences of seasonally oxic vs. anoxic hypolimnia for
269 biogeochemical cycling in an ecosystem model. These highly contrasting scenarios were
270 achieved in the model by manipulating hypolimnetic oxygen injection (described below).
271 Second, to determine the cumulative fate of C, N, and P over an entire summer in response to
272 oxygen dynamics, it is important to track these elements at a high temporal resolution. Because
273 our field data were collected weekly to monthly, we used numerical modeling of hydrodynamics
274 and ecosystem processes to capture daily dynamics. Third, the field manipulation included a
275 variable oxygenation schedule which occurred against a backdrop of changing meteorology and
276 hydrology. Consequently, the model enabled us to isolate the effects of oxygen availability on
277 the reservoir's biogeochemistry and evaluate the robustness of ecosystem responses across
278 varying environmental conditions.

279

280 *Model configuration and calibration*

281 All GLM-AED model configuration files, parameters, and driver data for FCR are
282 available in the EDI repository (Carey et al. 2021c). GLM-AED driver data included hourly
283 meteorological data from NASA's North American Land Data Assimilation System (NLDAS-2;
284 Xia et al. 2012), stream inflow data, and outflow data. We developed stream inflow driver
285 datasets – which consisted of daily discharge, water temperature, and chemistry – for the two
286 primary streams entering FCR from observational data (Supplementary Text 3). To simulate the
287 HOx system in the model, we added a submerged inflow that injected oxygenated water into the
288 reservoir at 8 m, the same depth as in the reservoir (Supplementary Text 3). As the reservoir was
289 managed to keep constant water level, outflow volume was set to equal inflow volume; the

290 physical and chemical properties of the outflow were determined by the state of the modeled
291 reservoir (Supplementary Text 3).

292 We ran the model from 15 May 2013 to 31 December 2019, divided into calibration (15
293 May 2013-31 December 2018) and validation (1 January 2019-31 December 2019) periods for
294 model verification. GLM-AED was run on an hourly time step throughout the total simulation
295 period (Carey et al. 2021c).

296 We calibrated GLM-AED to observed conditions (Supplementary Text 3). First, we
297 conducted a global sensitivity analysis to identify the most important parameters for simulating
298 water temperature, dissolved oxygen, NH_4^+ , NO_3^- , DRP, and DOC following Morris (1991).
299 Second, we calibrated the identified sensitive parameters (Supplementary Text 3) using the
300 covariance matrix adaptation evolution strategy for automated numerical optimization to
301 minimize root mean square error (RMSE) between observations and model output (Hansen
302 2016) for all sampling depths in the water column.

303 We calculated multiple goodness-of-fit metrics to assess the model's performance during
304 the calibration period, validation period, and total simulation period, including RMSE, the
305 coefficient of determination (R^2), percent bias, and normalized mean absolute error (NMAE)
306 (e.g., Kara et al. 2012, Ward et al. 2020, Ladwig et al. 2021). We calculated these goodness-of-
307 fit metrics following the most common approaches used in 328 recent freshwater modeling
308 studies (reviewed by Soares and Calijuri 2021; described in Supplementary Text 3).

309

310 *Model scenarios*

311 Following model calibration, we examined the effects of two different oxygen scenarios
312 on the calibrated GLM-AED model: one in which the model was forced with a high level of

313 oxygenation to keep the hypolimnion oxic throughout summer thermal stratification (May 15-
314 Oct 15) during 2013-2019 and one in which zero oxygen was added to the hypolimnion, so
315 hypolimnetic anoxia quickly set up after the onset of thermal stratification each summer. All
316 other driver data (meteorology, stream inflows, outflow) were held constant.

317

318 *Statistical analysis*

319 We used several approaches to answer the two research questions. For Q1, we first
320 compared observed data from the oxygenated vs. non-oxygenated periods of our field
321 manipulation to determine if oxygenation had an effect on empirical total and dissolved C, N,
322 and P concentrations. We pooled all hypolimnetic C, N, and P samples from the two summers
323 with the least oxygenation (July 15 - October 1 in 2018, 2019) when the HOx was deactivated
324 and compared them with concentrations measured during the two summers with the most
325 continuous oxygenation (July 15 - October 1 in 2016, 2017) when the HOx was activated. We
326 also used the FCR field data to validate the model's ability to simulate the field manipulation.
327 Second, because our goal was to compare completely oxic vs. completely anoxic summers and
328 every summer had at least some oxygenation during the seven-year field manipulation, we
329 focused our subsequent analyses on the anoxic vs. oxic model scenario output, which provided
330 complementary data to the non-oxygenated vs. oxygenated empirical data. Focusing on the
331 model output for this analysis also enabled us to overcome the limitations of comparing years
332 with different numbers of sampling observations, as the model calculated daily C, N, and P
333 concentrations and rates.

334 We compared hypolimnetic C, N, and P concentrations and rates between the oxic and
335 anoxic model scenarios during 15 July - 1 October among years, the interval within the summer

336 thermally stratified period when the reservoir consistently exhibited hypolimnetic anoxia in non-
337 oxygenated conditions. We calculated the median hypolimnetic dissolved and total
338 concentrations of C, N, and P during this period for each of the seven years (2013-2019), and
339 compared the median summer anoxic and oxic concentrations and their ratios using paired t-
340 tests, as there was no temporal autocorrelation among median summer values. We also examined
341 summer rates of all processes controlling increases and decreases in hypolimnetic C, N, and P to
342 determine their relative importance and sensitivity to oxygen.

343 To examine how the uncertainty of our model outputs was affected by the model
344 parameterization, we conducted an additional sensitivity analysis in which we doubled and
345 halved the calibrated values of highly sensitive parameters for DOC, NH_4^+ , NO_3^- , and DRP using
346 a one-step-at-a-time (OAT) approach (following Brett et al. 2016). We then re-calculated the
347 summer hypolimnetic concentrations of DOC, NH_4^+ , NO_3^- , and DRP in the anoxic and oxic
348 model scenarios for each variable and compared anoxic and oxic concentrations with paired t-
349 tests, as described above.

350 For Q2, we estimated C, N, and P downstream export as a percent of inputs into the
351 reservoir each summer (Powers et al. 2015, Farrell et al. 2020). Downstream export was
352 calculated as:

$$353 \textit{Flux} = 100\% \times ((\Sigma \textit{Outputs} - \Sigma \textit{Inputs}) / \Sigma \textit{Inputs}) \quad (\text{eqn. 1})$$

354 where Outputs and Inputs represent the daily mass of C, N, or P leaving and entering the
355 reservoir, respectively, during 15 July - 1 October each year. Fluxes were calculated for both
356 dissolved and total fractions of C, N, and P. Inputs were calculated by multiplying the individual
357 stream daily inflow concentrations with their daily inflow volumes and then summing across the
358 two streams. Outputs were calculated by multiplying the outflow water volume (leaving the

359 reservoir and going downstream) by hypolimnetic concentrations. A water budget calculated for
360 the reservoir in 2014-2015 (Munger et al. 2019) supplemented by monitoring data in this study
361 indicates that the two inflow streams represented approximately 97% of the reservoir's water
362 inputs (Supplementary Text 1), motivating our focus on those inputs.

363 Inputs and Outputs were summed across the 15 July - 1 October period to calculate C, N,
364 and P fluxes. Flux values of 0 indicated that the reservoir inputs balanced outputs; flux values <0
365 indicated that the reservoir was a net sink of C, N, or P; and flux values >0 indicated that the
366 reservoir was a net source of C, N, or P downstream. We compared summer retention (i.e., flux
367 values) in the anoxic and oxic scenarios with paired t-tests.

368 To ease comparison among C, N, and P concentrations and ratios, all analyses were
369 conducted in molar units. All analyses were conducted in R v.3.6.3 (R Core Team 2020).

370

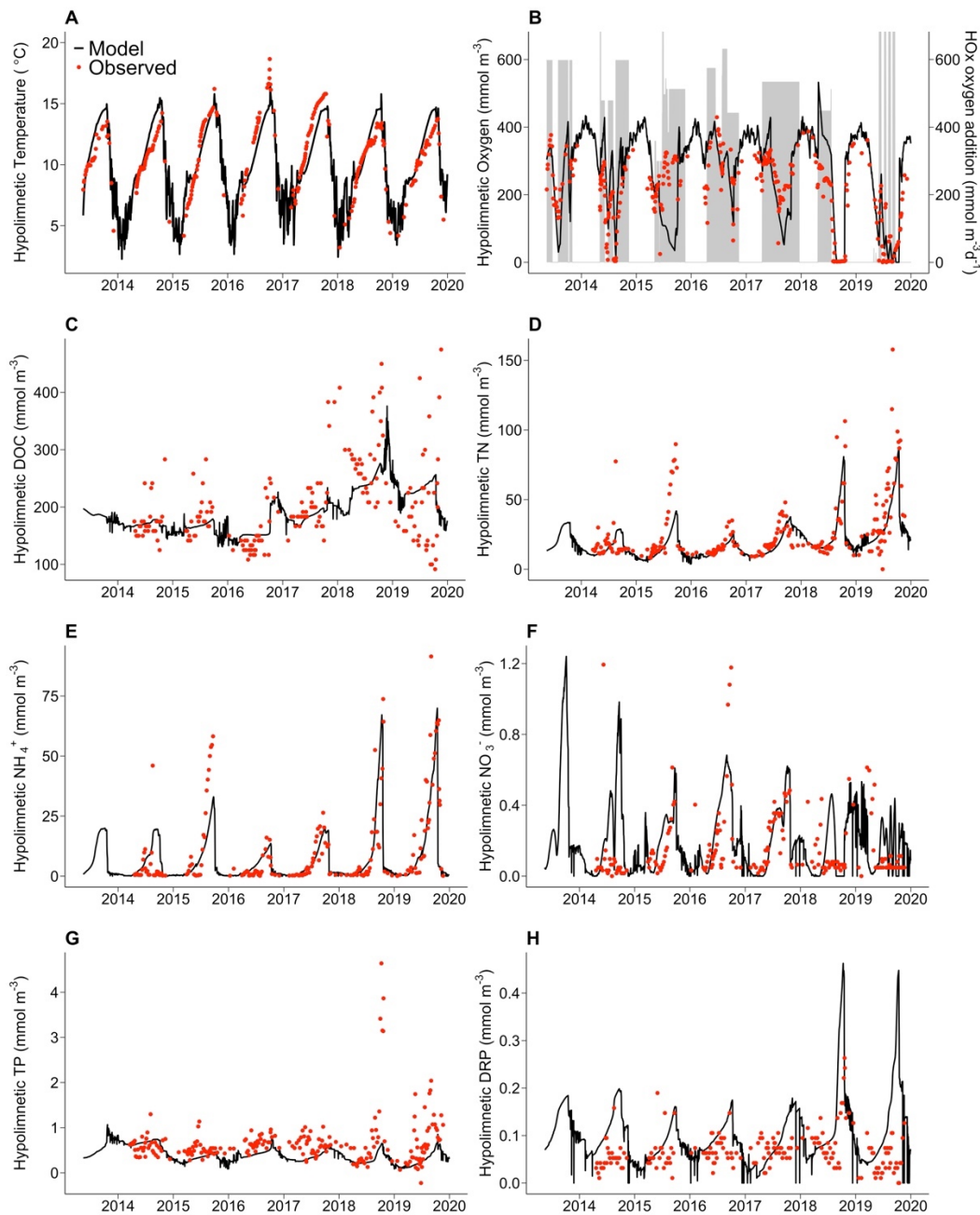
371 **Results**

372 Our integrated whole-ecosystem REDOX field manipulation and modeling demonstrates
373 that hypolimnetic anoxia significantly alters water column C, N, and P concentrations and
374 stoichiometry. Importantly, our study also shows that prolonged hypolimnetic anoxia in the
375 summer decreases the ability of a reservoir to retain C, N, and P, substantially increasing its
376 downstream export.

377

378 *Observational data from whole-ecosystem manipulations*

379 Injection of oxygen into the bottom waters of Falling Creek Reservoir (FCR) over seven
380 years increased the reservoir's observed hypolimnetic oxygen, resulting in substantial changes in
381 total and dissolved C, N, and P concentrations (Fig. 3, Fig. S2). Due to the nature of our



382
 383
 384
 385
 386
 387
 388
 389
 390
 391
 392
 393

Fig. 3. The model was able to generally recreate observed reservoir dynamics. Modeled (black line) and observed (red points) hypolimnetic (9 m) water temperature (A), dissolved oxygen (B), dissolved organic carbon (DOC; C), total nitrogen (TN; D), ammonium (NH₄⁺; E), nitrate (NO₃⁻; F), total phosphorus (TP; G), and dissolved reactive phosphorus (DRP; H) in Falling Creek Reservoir (goodness-of-fit metrics presented for the full water column in Table 1). The grey shaded areas in panel B represent the periods and addition rates of oxygen injection into the hypolimnion from the hypolimnetic oxygenation system (HOx) during the seven-year field manipulation. Note varying y-axes among panels, and that many of the NO₃⁻ and DRP observations were below the limit of quantitation in laboratory analysis (0.11 and 0.08 mmol m⁻³, respectively).

394 oxygenation manipulation, some years experienced low levels of oxygenation (i.e., the HOx was
395 off for prolonged periods throughout the summer), while others experienced high levels of
396 oxygenation during the stratified period (Fig. 3B). Oxygenation resulted in substantially higher
397 hypolimnetic oxygen concentrations without altering water temperature and thermal stratification
398 in the reservoir (Fig. 3A,B). In 2019, oxygenation did not increase hypolimnetic oxygen
399 concentrations to the same extent as preceding summers, likely because the HOx was only
400 operated for intermittent 2-week periods (vs. 4-week or longer periods in all other years).

401 The median observed hypolimnetic DOC, NH_4^+ , and DRP concentrations were 2.0, 6.9,
402 and $1.3\times$ higher in the summers with the least oxygenation (2018, 2019) than in the summers
403 with the highest oxygenation (2016, 2017; Fig. 3C,E,H; Fig. S2), respectively. Following the
404 patterns exhibited by the dissolved fractions, median observed hypolimnetic TN and TP
405 concentrations were both $2.4\times$ higher in the high vs. low oxygenation summers (Fig. 3D,G; Fig.
406 S2). Conversely, median observed hypolimnetic NO_3^- concentrations were $5\times$ lower in summers
407 with low oxygenation than summers with high oxygenation (Fig. 3F, Fig. S2). Because our goal
408 was to compare completely oxic vs. completely anoxic summer conditions and every summer
409 had at least some oxygenation during the seven-year field manipulation at varying levels of
410 oxygen injection, subsequent analyses focused on the anoxic vs. oxic model scenario output,
411 described below.

412

413 *Model performance*

414 The field manipulation data were used to calibrate the ecosystem model, which generally
415 reproduced observed water temperature, oxygen, dissolved and total C, N, and P concentrations,
416 and stoichiometry (Table 1, Fig. 3, Supplementary Text 4). Similar to field observations, the

417 **Table 1. Goodness-of-fit (GOF) metrics for comparing observations and modeled GLM-**
 418 **AED output for Falling Creek Reservoir, VA, USA.** GOF metrics include root mean square
 419 error (RMSE), percent bias (PBIAS%), coefficient of determination (R^2), and normalized mean
 420 absolute error (NMAE); n is the number of observed measurements. Each GOF metric was
 421 calculated comparing model outputs and observational data for the water column for the Full
 422 simulation (2013-2019); Calibration (2013-2018); and Validation (2018-2019); see
 423 Supplementary Text 3 for details. Evaluated parameters include temperature (Temp, °C), summer
 424 thermocline depth (TD, m), dissolved oxygen (mmol m^{-3}), dissolved organic carbon (DOC,
 425 mmol m^{-3}), total nitrogen (TN, mmol m^{-3}), ammonium (NH_4^+ , mmol m^{-3}), nitrate (NO_3^- , mmol
 426 m^{-3}), total phosphorus (TP, mmol m^{-3}), and dissolved reactive phosphorus (DRP, mmol m^{-3}).

Time period	Parameter	Temp	TD	Oxygen	DOC	TN	NH₄⁺	NO₃⁻	TP	DRP
Full simulation	n	3639	324	3726	1277	1518	1277	1485	1724	1271
	RMSE	1.41	0.8	49.1	63.2	5.9	2.81	0.16	0.29	0.05
	PBIAS%	4.4	0.1	6.4	-14.5	-6.2	22.5	9.8	-31.7	26.5
	R^2	0.95	0.50	0.72	0.30	0.71	0.77	0.27	0.25	0.10
Calibration	NMAE	0.09	0.18	0.15	0.2	0.22	0.46	0.45	0.38	0.37
	n	3164	284	3251	1018	1250	1018	1014	1456	1012
	RMSE	1.39	0.9	45.9	61.5	5.0	2.81	0.16	0.25	0.04
	PBIAS%	3.3	-1.4	5.8	-16.8	-0.8	40.7	11.7	-29.6	21.1
Validation	R^2	0.95	0.46	0.71	0.46	0.58	0.63	0.33	0.15	0.24
	NMAE	0.09	0.19	0.14	0.19	0.19	0.61	0.44	0.33	0.28
	n	475	40	475	259	268	259	471	268	259
	RMSE	1.48	0.4	62.8	70.4	9.23	2.79	0.14	0.33	0.08
	PBIAS%	11.2	10.5	9.9	-4.2	-19.8	-7.2	3.3	-42.9	51.6
Validation	R^2	0.97	0.95	0.74	0.52	0.94	0.94	0.12	0.85	0.03
	NMAE	0.12	0.1	0.2	0.24	0.36	0.22	0.49	0.38	0.57

427

428 simulation of oxygen injection in the model did not substantively alter modeled water
429 temperature or thermocline depth (Table 1, Fig. 3A).

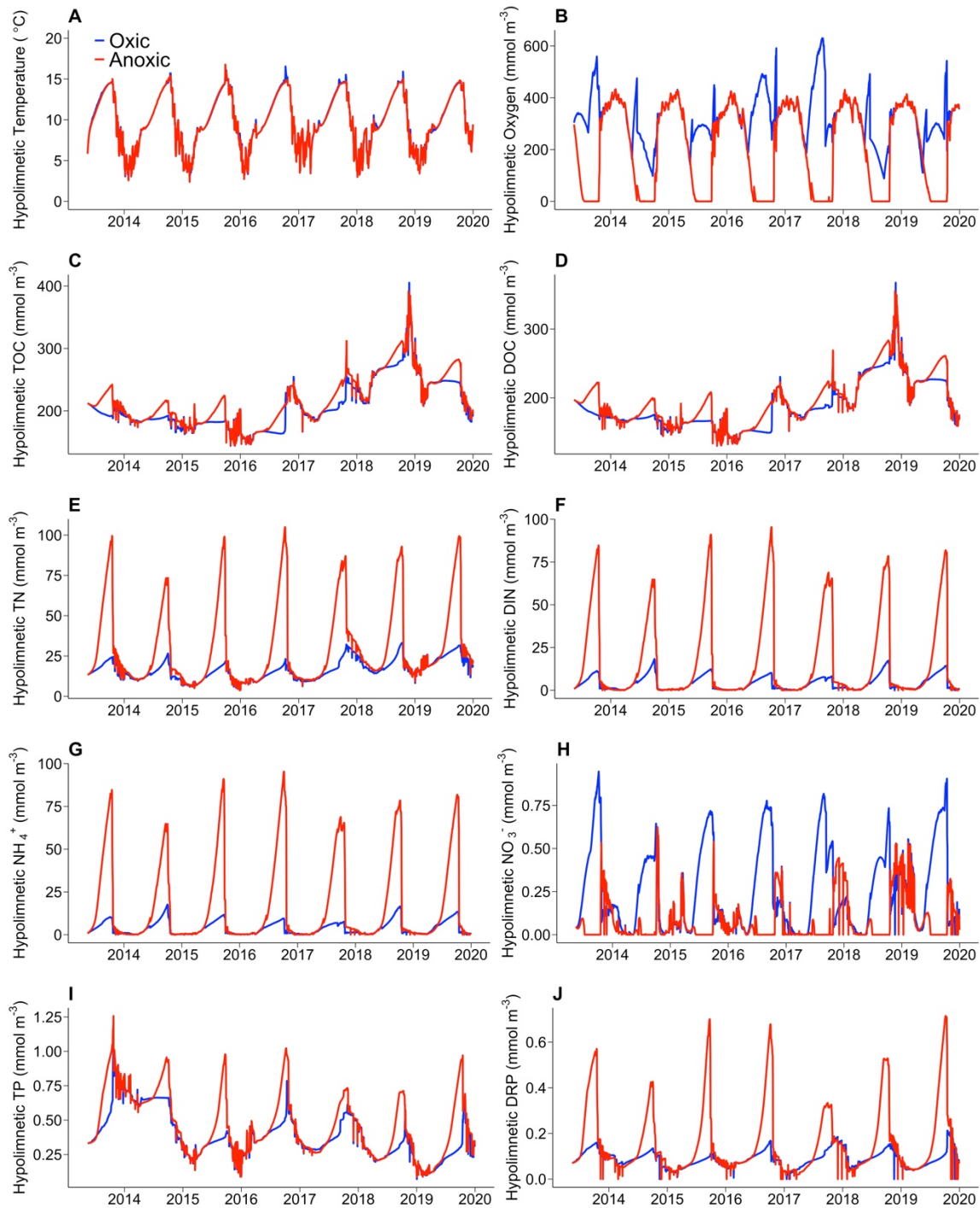
430 Model performance of most state variables in our study (Table 1) exceeded the median
431 goodness-of-fit metrics for recent freshwater modeling studies reported by Soares and Calijuri
432 (2021). For example, our water temperature R^2 was 0.95 for the full seven-year simulation period
433 (vs. 0.94 in Soares and Calijuri 2021), our dissolved oxygen R^2 was 0.72 (vs. 0.61), our TN was
434 0.71 (vs. 0.61), and our NH_4^+ R^2 was 0.77 (vs. 0.35). No DOC data were reported by Soares and
435 Calijuri (2021), but our R^2 values ranged from 0.30-0.52 for the full simulation, calibration, and
436 validation periods. Phosphorus had less good fit, but was still reasonable: our TP R^2 was 0.25 for
437 the full seven-year simulation period (slightly lower than the 0.30 reported by Soares and
438 Calijuri 2021), but the validation period's R^2 for TP was much higher, at 0.85. Similarly, our
439 DRP R^2 was 0.10 for the full seven-year period (vs. 0.32) but the six-year calibration period had
440 better performance, at an R^2 of 0.24. NO_3^- had an R^2 of 0.27 for the full seven-year modeling
441 period and R^2 of 0.33 for the six-year calibration period, which was lower than the 0.61 reported
442 by Soares and Calijuri (2021).

443 Much of the variation in DRP and NO_3^- observations was within the analytical limits of
444 quantitation. Consequently, while the model generally captured seasonal patterns of DRP and
445 NO_3^- , it was simply not possible to reproduce short-term fluctuations in observations below
446 method detection limits. NO_3^- concentrations in particular were extremely low in both field
447 observations and model output (Fig. 3F). Throughout the study, NO_3^- was a very minor fraction
448 of TN, representing a median of 0.5% ($\pm 0.9\%$, 1 S.D.) of TN at all depths in the field data and a
449 median of 0.8% ($\pm 0.9\%$) of TN in the baseline simulation. Subsequently, a lower fit of NO_3^- did
450 not affect the model performance of TN, as evident by its goodness-of-fit metrics (Table 1).

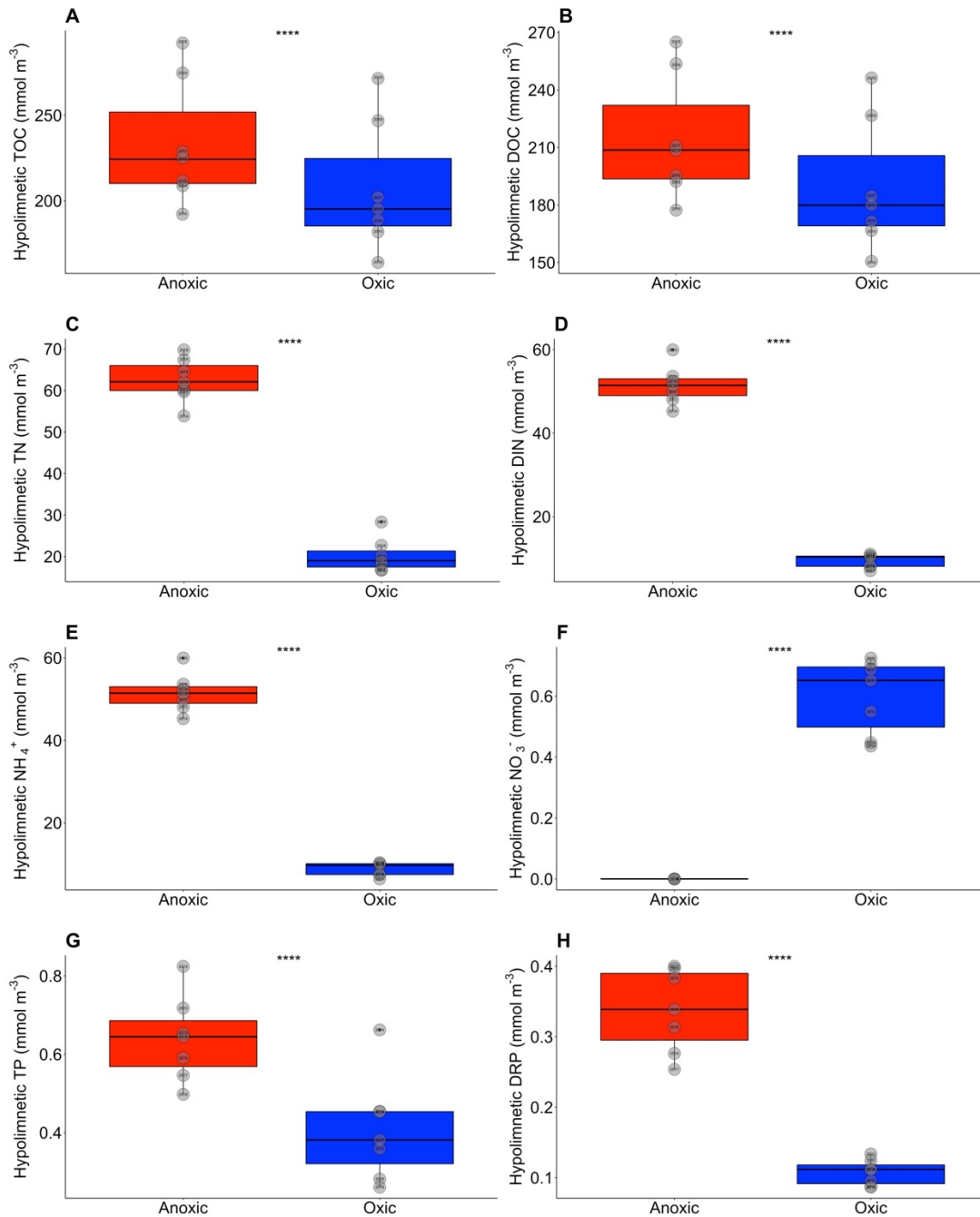
451 *How does hypolimnetic oxygen availability affect total and dissolved C, N, and P concentrations*
452 *and stoichiometry?*

453 Model scenarios show that hypolimnetic anoxia significantly affected all three focal
454 elemental cycles, but that N was the most sensitive (Figs. 4,5; see Table S3 for statistics).
455 Summer TN molar concentrations in the reservoir were on average 3.0× higher in anoxic than
456 oxic conditions, relative to a 1.1× increase of TOC and 1.6× increase of TP (Fig. 5A,C,G). The
457 dissolved fractions accounted for most of the changes in total C, N, and P: following the field
458 data, modeled summer hypolimnetic DOC, NH_4^+ , and DRP concentrations in FCR were on
459 average 1.1, 5.8, and 3.1× higher, respectively, during anoxic conditions than in oxic conditions
460 (Fig. 5B,E,H). Conversely, hypolimnetic NO_3^- was much lower in anoxic conditions (usually at
461 or just above 0 mmol m^{-3}) than oxic conditions, but DIN exhibited an overall increase because of
462 the dominance of NH_4^+ over NO_3^- in the dissolved inorganic N pool (Fig. 5D,F). The statistical
463 significance and overall magnitude of differences in concentrations between the anoxic and oxic
464 scenarios were consistent even when focal parameters governing DOC, NH_4^+ , NO_3^- , and DRP
465 were doubled or halved in the parameter sensitivity analysis (Supplementary Text 3, Fig. S1).

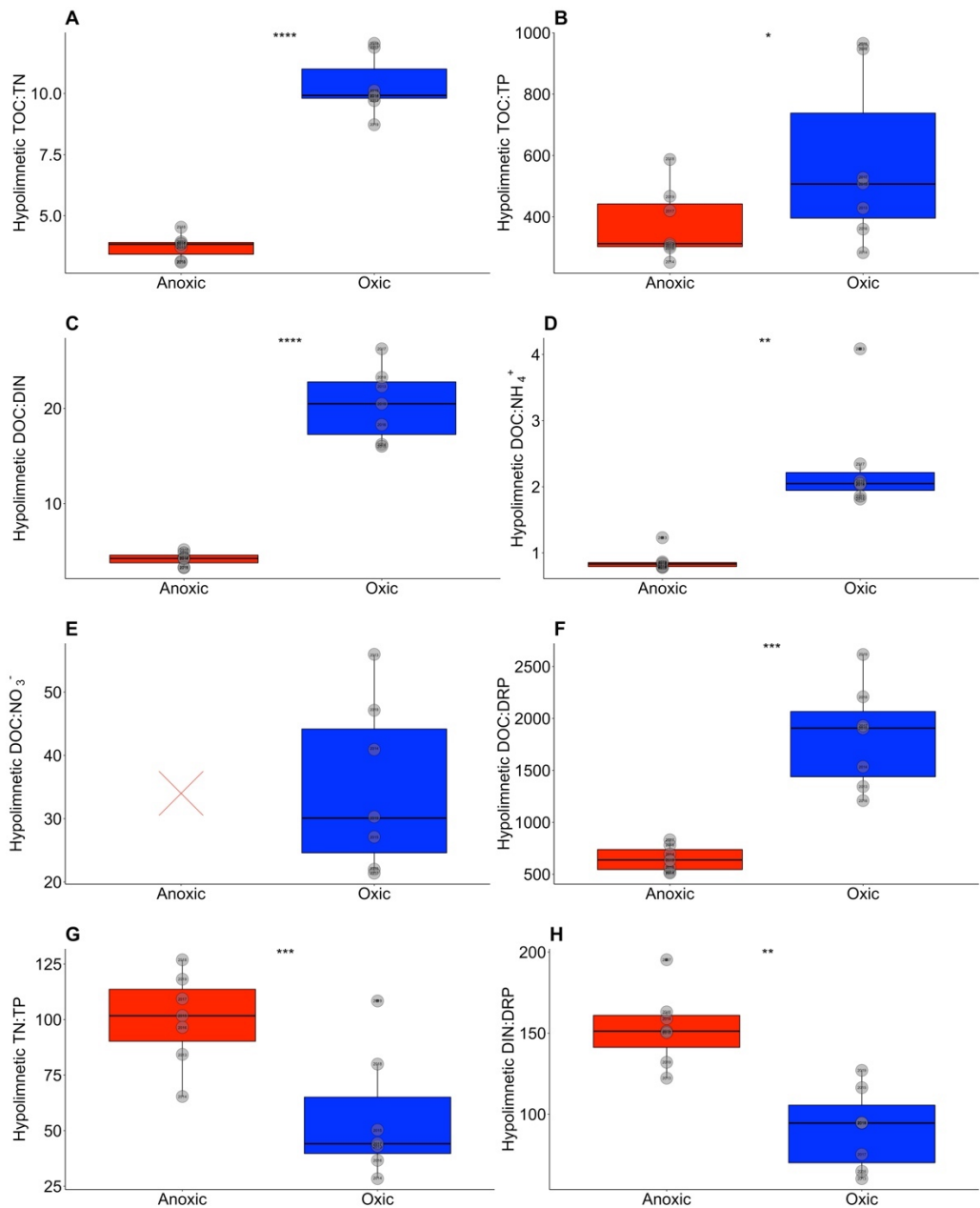
466 The elemental stoichiometry in FCR exhibited rapid and large ecosystem-scale changes
467 after the onset of anoxia each summer. While total and dissolved fractions of C, N, and P (except
468 NO_3^-) significantly increased with anoxia (Figs. 4,5), the different fractions had varying
469 sensitivities to changing oxygen, resulting in significant changes in C, N, and P ratios (Fig. 6,
470 Supplementary Text 5). Hypolimnetic TN:TP and DIN:DRP were significantly higher (both by
471 1.9×, on average) in anoxic conditions than oxic conditions (Fig. 6G,H). Because modeled
472 hypolimnetic NO_3^- concentrations were at or near zero during anoxic conditions (Fig. 5F),
473 DOC: NO_3^- could not be consistently calculated (Fig. 6E). In contrast, TOC:TN, TOC:TP,
474



475
 476 **Fig. 4. Time series of oxic (blue) and anoxic (red) model scenarios in Falling Creek**
 477 **Reservoir.** Model results are shown for hypolimnetic (9 m) water temperature (A), dissolved
 478 oxygen (B), total organic carbon (TOC; C), dissolved organic carbon (DOC; D), total nitrogen
 479 (TN; E), dissolved inorganic nitrogen (DIN, the sum of ammonium and nitrate; F), ammonium
 480 (NH_4^+ ; G), nitrate (NO_3^- ; H), total phosphorus (TP; I), and dissolved reactive phosphorus (DRP;
 481 J). In the oxic scenario, oxygen was injected into the hypolimnion throughout the thermally
 482 stratified period each summer. In the anoxic scenario, no oxygen was added to the hypolimnion,
 483 resulting in prolonged hypolimnetic anoxia each summer. Note varying y-axes among panels.



484
 485 **Fig. 5. Anoxia significantly altered bottom-water concentrations of carbon, nitrogen, and**
 486 **phosphorus.** Median hypolimnetic (9 m) total organic carbon (TOC; A), dissolved organic
 487 carbon (DOC; B), total nitrogen (TN; C), dissolved inorganic nitrogen (DIN; D), ammonium
 488 (NH₄⁺; E), nitrate (NO₃⁻; F), total phosphorus (TP; G), and dissolved reactive phosphorus (DRP;
 489 H) concentrations between anoxic (red) and oxic (blue) scenarios during Falling Creek
 490 Reservoir's stratified period (July 15 - October 1) for all years of this study. The grey points are
 491 the median values from each of the seven years. The **** denotes that the difference between
 492 the median summer anoxic and oxic scenario concentrations was highly statistically significant
 493 (all paired t-tests $p \leq 0.0001$, see Supplementary Text 5 and Table S3 for statistics). Note varying
 494 y-axes among panels.

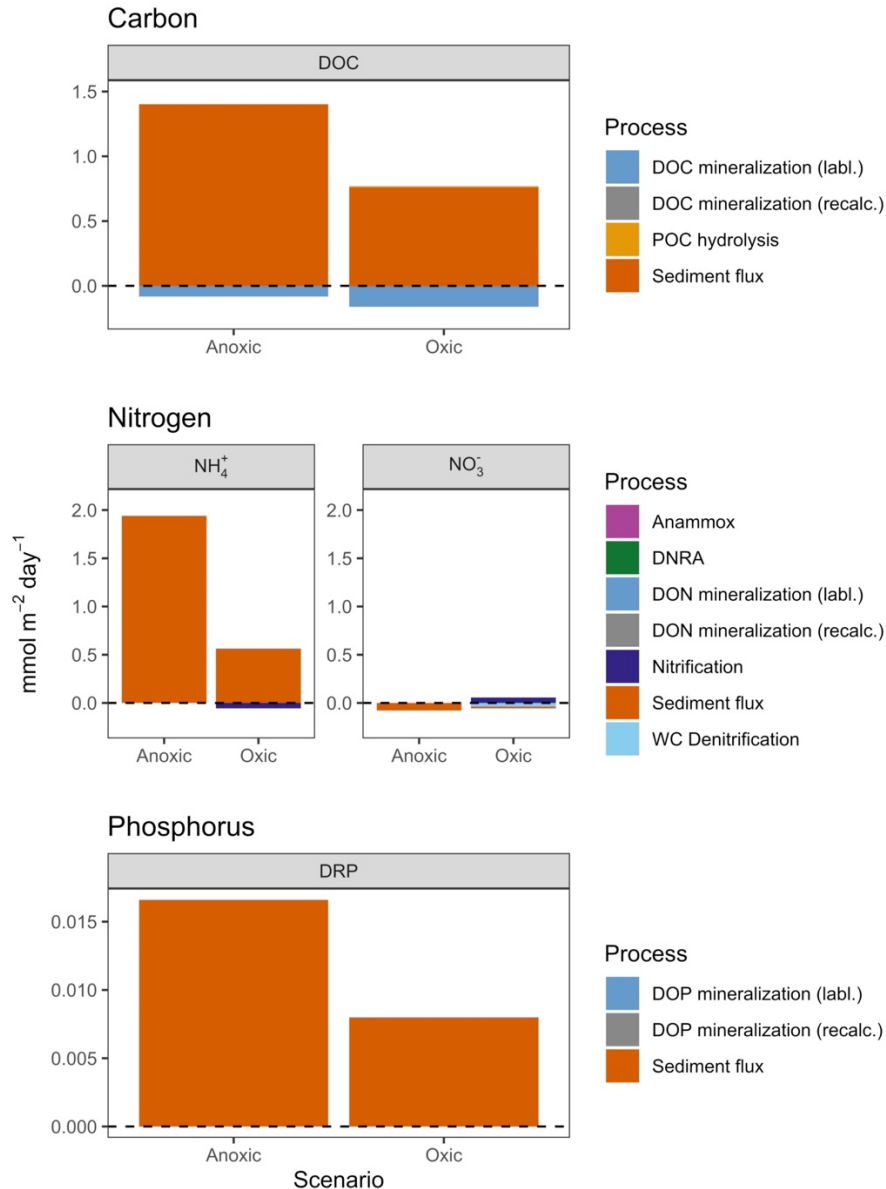


495
 496 **Fig. 6. Anoxia significantly affected water column stoichiometry.** Total and dissolved molar
 497 ratios of hypolimnetic (9 m) total organic carbon:total nitrogen (TOC:TN; A), TOC:total
 498 phosphorus (TOC:TP; B), dissolved organic carbon:dissolved inorganic nitrogen (DOC:DIN; C),
 499 DOC:ammonium (DOC:NH₄⁺; D), DOC:nitrate (DOC:NO₃⁻; E), DOC:dissolved reactive
 500 phosphorus (DOC:DRP; F), TN:TP (G), and DIN:DRP (H) between anoxic (red) and oxic (blue)
 501 scenarios during Falling Creek Reservoir's stratified period (July 15 - October 1) for all years of
 502 this study. The grey points are the median values from each of the seven years. Because NO₃⁻
 503 concentrations in the anoxic scenario were functionally zero, the ratio of DOC:NO₃⁻ could not be
 504 calculated (hence the X in panel E). The asterisks denote the p-values from paired t-tests
 505 comparing the median summer ratios between anoxic and oxic scenarios: **** p < 0.0001, *** p
 506 < 0.001, ** p < 0.01, and * p < 0.05 (see Supplementary Text 5 and Table S4 for statistics). Note
 507 varying y-axes among panels.

508 DOC:DIN, DOC:NH₄⁺, and DOC:DRP were significantly higher (on average, by 2.7×, 0.7×,
509 4.7×, 5.0×, and 2.7×, respectively) in oxic conditions than anoxic conditions (Fig. 6A,B,C,D,F,
510 Supplementary Text 5).

511 The most important processes driving the biogeochemical responses to anoxia were much
512 higher fluxes of NH₄⁺, DRP, and DOC into the hypolimnion from the sediments in anoxic
513 periods relative to oxic periods (Fig. 7). During anoxic summer conditions, the median release
514 rates of NH₄⁺ and DRP from the sediments into the water column were 3.6× and 2.2× higher,
515 respectively, than in oxic conditions (Fig. 7). During oxic conditions, the sediment release rate of
516 NH₄⁺ into the hypolimnion was 34× greater than the consumption of NH₄⁺ by nitrification (Fig.
517 7, Fig. S5), thereby explaining the hypolimnetic accumulation of NH₄⁺ that occurred during oxic
518 conditions (Fig. 4G). Although median labile dissolved organic N (DON) and P (DOP)
519 mineralization rates were both 4.0× times higher in oxic than anoxic conditions, their
520 contribution to hypolimnetic N and P budgets was much smaller than NH₄⁺ and DRP sediment
521 fluxes. All biogeochemical rates involving the cycling of NO₃⁻ were much lower than for NH₄⁺
522 overall, likely because of the much lower concentrations of NO₃⁻ within the DIN pool. For DOC,
523 the median sediment fluxes increasing DOC in the hypolimnion were 1.9× times higher in anoxic
524 than oxic conditions. Although labile DOC mineralization rates were 2.0× higher in oxic than
525 anoxic conditions, sediment flux rates were 19× higher than mineralization rates, resulting in
526 much greater hypolimnetic accumulation of DOC in anoxic relative to oxic periods (Fig. 7).

527 The time scales at which C, N, and P concentrations responded to shifts in hypolimnetic
528 oxygen availability differed as a result of multiple interacting biogeochemical processes (Figs.
529 4,7). For example, the onset of anoxia each summer triggered rapid decreases in NO₃⁻ (Fig. 4H),
530 due to sediment denitrification oxidizing NO₃⁻ to N₂ (Fig. 7). Similarly, the rapid increases in

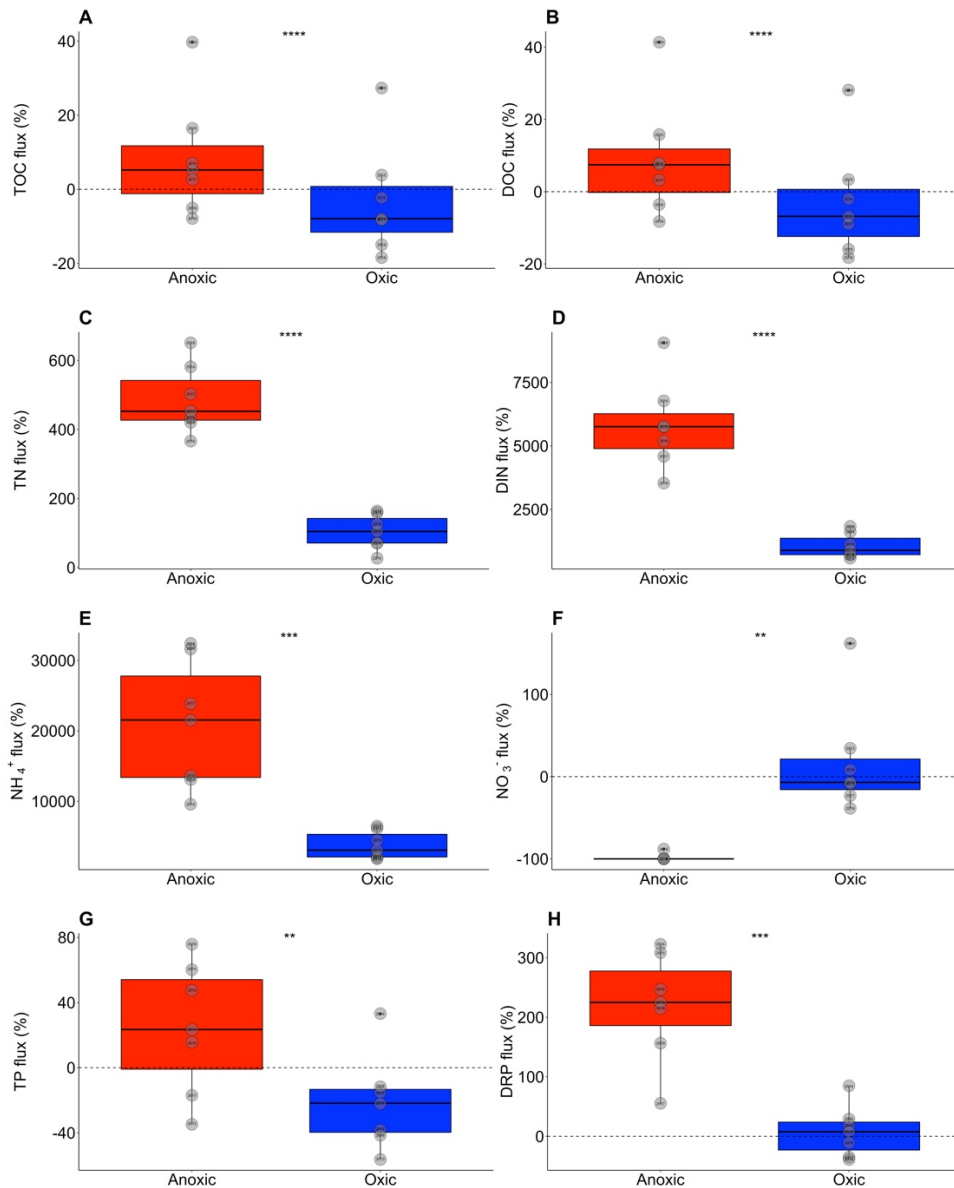


531
 532 **Fig. 7. Sediment fluxes dominated the biogeochemical cycling of dissolved carbon, nitrogen,**
 533 **and phosphorus and their responses to anoxia.** Comparison of the dominant biogeochemical
 534 processes altering dissolved pools of carbon (dissolved organic carbon, DOC; top), nitrogen
 535 (ammonium, NH_4^+ , and nitrate, NO_3^- ; middle), and phosphorus (dissolved reactive phosphorus,
 536 DRP; bottom) in the hypolimnion of Falling Creek Reservoir under anoxic vs. oxic model
 537 scenarios. Rates shown represent the median contribution of each process to hypolimnetic
 538 concentrations of DOC, NH_4^+ , NO_3^- , and DRP during Falling Creek Reservoir's summer
 539 stratified period (July 15 - October 1) for all years of this study. Positive rates indicate that the
 540 process increased hypolimnetic concentrations; negative rates indicate that the process decreased
 541 hypolimnetic concentrations. Mineralization is shown separately for both labile (labl.) and
 542 recalcitrant (recalc.) dissolved organic pools, and denitrification is partitioned for the water
 543 column (WC Denitrification) and sediment in the NO_3^- panel (Sediment flux). Note the varying
 544 y-axes among panels and that some rates are so small that they are not visible in the figure; Fig.
 545 S5 shows a modified version of this figure with the sediment fluxes excluded.

546 hypolimnetic NH_4^+ and DOC concentrations after the onset of anoxia (Fig. 4D,G) were
547 attributable to the high rates of NH_4^+ and DOC sediment release (Fig. 7). In comparison,
548 hypolimnetic DRP accumulation in response to anoxia occurred more slowly (Fig. 4J). This
549 difference in time scale reflects the lower fitted value of the half-saturation constant of modeled
550 DRP sediment fluxes (6.91 mmol m^{-3}) relative to the half-saturation constants of NH_4^+ sediment
551 fluxes ($41.25 \text{ mmol m}^{-3}$) and DOC sediment fluxes ($93.13 \text{ mmol m}^{-3}$; Carey et al. 2021c).
552 Consequently, oxygen concentrations in the hypolimnion had to decrease to near zero before
553 anoxia stimulated an increase in DRP sediment fluxes, following Michaelis-Menten dynamics.
554

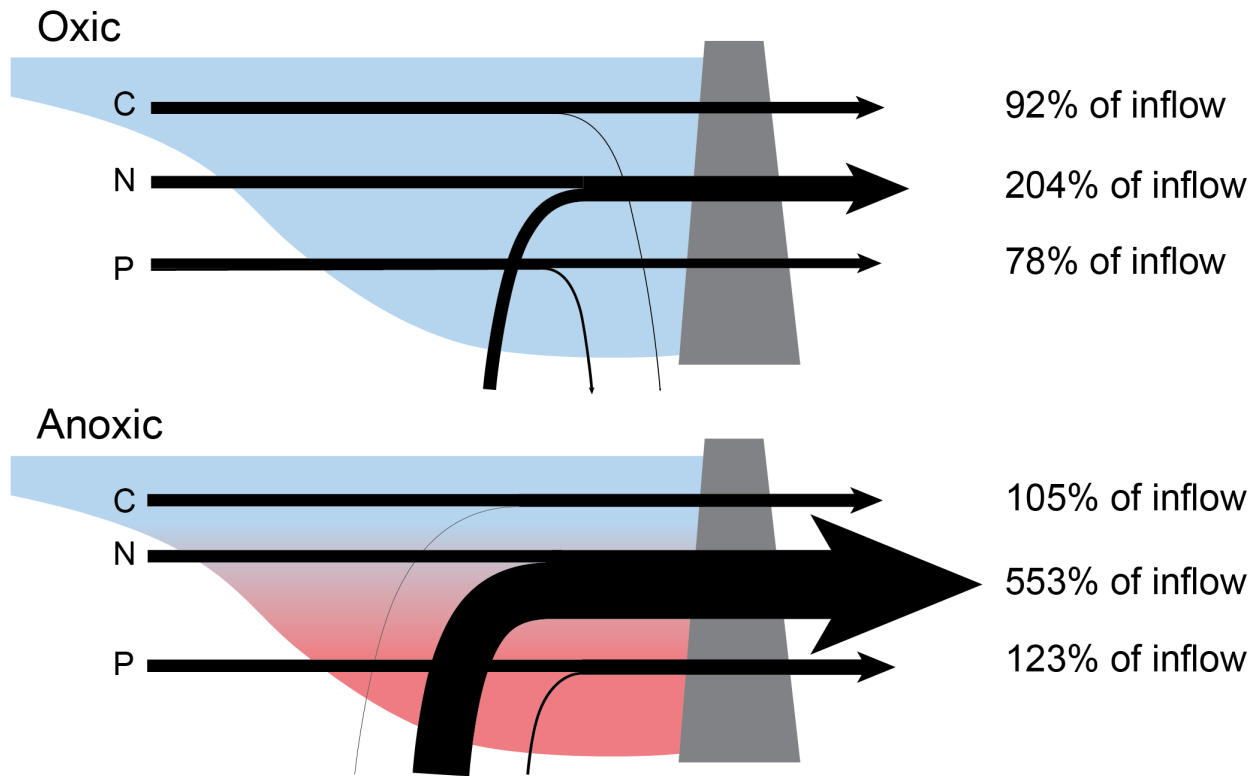
555 *How does hypolimnetic anoxia affect reservoir downstream export of C, N, and P?*

556 Overall, anoxia significantly increased downstream export of C, N, and P from FCR (Fig.
557 8). During the summer months, if the reservoir's hypolimnion was oxic, FCR served as a net sink
558 for inflowing TOC and TP, decreasing the downstream export of those fractions (Fig. 8A,G).
559 The reservoir served as a particularly important TP sink during summer oxic conditions, with
560 22% of inflowing TP buried in sediments, resulting in 78% of the inflowing TP exported
561 downstream (Fig. 9). In comparison, while the reservoir was also a TOC sink in oxic conditions,
562 only 8% of inflowing TOC was buried in sediments or removed via emission to the atmosphere,
563 resulting in 92% export downstream (Fig. 9). However, in most anoxic summers, the reservoir
564 became a net source of TOC and TP downstream, meaning that inflowing TOC and TP - as well
565 as TOC and TP that were previously retained in the reservoir sediments - were released and
566 transported out of the reservoir (Fig. 8A,G). Consequently, on average, the reservoir exported
567 105% of inflowing TOC and 123% of inflowing TP in anoxic conditions (Fig. 9). DOC and DRP
568 fluxes largely mirrored the patterns of the total fractions, though DRP had much greater flux



569

570 **Fig. 8. Anoxia significantly increased the downstream export of total and dissolved**
 571 **fractions of organic carbon, nitrogen, and phosphorus.** Percent downstream export (% flux)
 572 of total organic carbon (TOC; A), dissolved organic carbon (DOC; B), total nitrogen (TN; C),
 573 dissolved inorganic nitrogen (DIN; D), ammonium (NH_4^+ ; E), nitrate (NO_3^- ; F), total phosphorus
 574 (TP; G), and dissolved reactive phosphorus (DRP; H) inputs into Falling Creek Reservoir for
 575 anoxic (red) and oxic (blue) model scenarios during the stratified period (July 15 - October 1) for
 576 all years of this study. Flux values of 0 (denoted by dashed horizontal lines) indicated that the
 577 reservoir inputs balanced exports; flux values <0 indicated that the reservoir was a net sink of C,
 578 N, or P; and flux values >0 indicated that the reservoir was a net source of C, N, or P
 579 downstream. The grey points are the median values from each of the seven years. The asterisks
 580 denote the p-values from paired t-tests comparing the median summer retention in anoxic and
 581 oxic scenarios: **** $p < 0.0001$, *** $p < 0.001$, and ** $p < 0.01$ (see Supplementary Text 5 and
 582 Table S5 for statistics). Note varying y-axes among panels.



583

584 **Fig. 9. Median summer downstream export of total organic carbon (C), total nitrogen (N),**
 585 **and total phosphorus (P) inputs under oxic (top) and anoxic (bottom) conditions.** The “% of
 586 inflow” value represents the percent of inflowing C, N, and P into the reservoir that is exported
 587 downstream. A value of 100% indicates that reservoir inputs balanced exports; values <100%
 588 indicated that the reservoir was a net sink of C, N, or P; and values >100% indicated that the
 589 reservoir was a net source of C, N, or P downstream. Arrow widths are scaled to be proportional
 590 to the median downstream export of each element.
 591

592 downstream overall in anoxic summers than TP (Fig. 8B,H).

593 The reservoir was a net source of TN, DIN, and NH_4^+ downstream even in oxic
594 conditions, but this export significantly increased when the hypolimnion became anoxic in
595 summer (Fig. 8C,D,E). The only fraction of N that did not exhibit higher downstream export
596 during anoxic conditions was NO_3^- (Fig. 8F). During anoxic conditions, ~100% of inflowing
597 NO_3^- was removed due to sediment denitrification, whereas in oxic conditions, some of this NO_3^-
598 was exported downstream along with additional NO_3^- that originated from nitrified NH_4^+ in the
599 reservoir (Fig. 7). Overall, the reservoir exported 204% of inflowing TN in summer oxic
600 conditions and 553% in anoxic conditions (Fig. 9).

601 Aggregated across the seven years, FCR served as a small net sink of POC, PON, and
602 POP in its sediments in both oxic and anoxic model scenarios. All particulate organic fractions
603 exhibited significantly higher annual burial rates in anoxic scenarios than oxic scenarios, though
604 the differences were small, especially for POP (Supplementary Text 5, Table S6).

605

606 **Discussion**

607 Our study provides one of the first comprehensive analyses on the effects of oxygen on
608 multiple fractions of C, N, and P at the whole-ecosystem scale in a freshwater ecosystem. Our
609 unprecedented 7-year field manipulation coupled with ecosystem model simulations reveals that
610 anoxia may decrease the ability of reservoirs to serve as sinks of C, N, and P. Moreover, both the
611 empirical data and model output demonstrate that anoxia resulted in significantly higher summer
612 concentrations of hypolimnetic NH_4^+ , DRP, and DOC and altered dissolved and total
613 stoichiometry by factors of 2-5 \times . Our integrated field manipulation and modeling study provides
614 important insight on the biogeochemical cycling of these three elements, which are already

615 changing in many freshwaters globally due to human activities (Powers et al. 2015, Maranger et
616 al. 2018), and likely will change substantially more in the future as the prevalence and duration
617 of anoxia in lakes and reservoirs increase (Tranvik et al. 2009, North et al. 2014, Jenny et al.
618 2016a, Jane et al. 2021). Below, we first examine the effects of anoxia on each elemental cycle
619 separately, then their combined stoichiometry, and ultimately whole-ecosystem biogeochemical
620 processing and fate.

621

622 *Hypolimnetic carbon and nutrient chemistry*

623 This study provides an answer to the critical question of how increased anoxia will affect
624 OC cycling at the whole-ecosystem scale (Sobek et al. 2009, Brothers et al. 2014, Peter et al.
625 2016, Mendonça et al. 2017, Carey et al. 2018). The shift in reservoir OC cycling in response to
626 anoxia is the consequence of changes in three linked processes: POC burial, DOC
627 mineralization, and DOC release from the sediments. Under anoxic conditions, POC burial
628 increased slightly, DOC mineralization rates were low, and DOC release from the sediments to
629 the water column was 2× higher than in oxic conditions (Fig. 7, Fig. S5). Under oxic conditions,
630 DOC mineralization rates, while higher than in anoxic conditions (Fig. 7, Fig. S5), were still an
631 order of magnitude lower than the rate of hydrologic flushing. The net outcome of these three
632 processes was a substantial difference in OC retention in the reservoir during oxic vs. anoxic
633 conditions. Under oxic conditions, the reservoir served as a net sink of DOC and TOC, with up
634 to 18% of inflowing DOC and TOC retained in a summer (Fig. 8A,B). Under anoxic conditions,
635 the decrease in net retention of inflowing DOC and TOC more than offset the slight increase in
636 POC burial, and nearly all of the inflowing DOC and TOC was exported downstream (as
637 indicated by 0% or positive flux in Fig. 8A,B). In five of the seven years, FCR even became a

638 net exporter of TOC and DOC in the anoxic scenario (Fig. 8A,B), meaning that both inflowing
639 TOC and DOC and likely legacy TOC and DOC that were previously buried in sediments were
640 released and transported out of the reservoir.

641 The finding that anoxia simultaneously decreased the reservoir's role as a DOC sink yet
642 increased its role as a POC sink may explain some of the conflicting results that emerged from
643 previous studies that focused on only one OC fraction. First, our study supports past work that
644 observed increasing hypolimnetic DOC concentrations in anoxic conditions, suggesting that
645 anoxia decreases the freshwater OC sink (Brothers et al. 2014, Peter et al. 2016, Mendonça et al.
646 2017). The increasing hypolimnetic DOC concentrations have been attributed to both reductive
647 dissolution of iron-bound OC complexes in the sediments during anoxia (Skoog and Arias-
648 Esquivel 2009, Peter et al. 2016, Peter et al. 2017) and decreased mineralization rates in anoxic
649 conditions (Bastviken et al. 2004, Sobek et al. 2009). Our calibrated ecosystem model indicates
650 that both processes are important, but that the much higher hypolimnetic DOC concentrations in
651 anoxic conditions in FCR were primarily due to sediment release (Fig. 7). At the same time, our
652 work also supports laboratory microcosm and sediment core studies that observed lower POC
653 mineralization rates in anoxic than in oxic conditions (Bastviken et al. 2004, Sobek et al. 2009).
654 In FCR, mean summer POC hydrolysis rates in the hypolimnion were five orders of magnitude
655 lower in anoxic than oxic conditions (Fig. 7, Fig. S5), enabling slightly greater POC burial in
656 anoxic than oxic conditions. Altogether, our work indicates that using an ecosystem model to
657 simultaneously track both concentrations and rates of the major processes affecting dissolved,
658 particulate, and total pools of OC is needed to understand the full effects of oxygen on OC
659 cycling, as different fractions have different responses to anoxia.

660 Nitrogen was the most sensitive of the three focal elements to anoxia, with an NH_4^+ -
661 dominated TN budget that increased dramatically during anoxic conditions. The dominant
662 mechanism driving the NH_4^+ increase in anoxic conditions were the approximately 4× higher
663 rates of ammonification and sediment release than in oxic conditions (Fig. 7). Anammox and
664 nitrification rates were very low in anoxic conditions (Fig. 7, Fig. S5), enabling NH_4^+ to
665 accumulate in the hypolimnion during anoxia. In oxic conditions, nitrification rates were unable
666 to balance sediment fluxes, resulting in much lower but still noticeable increases in summer
667 NH_4^+ concentrations (Fig. 4G). As a result, the reservoir functioned as an NH_4^+ source
668 downstream regardless of hypolimnetic oxygen availability, though anoxia increased
669 downstream fluxes by 5× relative to oxic conditions, on average. The high sediment NH_4^+ fluxes
670 - even in oxic conditions - indicate that FCR has a large sediment NH_4^+ pool, which is likely due
671 to historical agriculture in the catchment (Gerling et al. 2016). Until agricultural abandonment in
672 the 1930s, most of FCR's catchment was farmland (Gerling et al. 2016). Even though the
673 catchment did not experience industrial farming, agriculture can have century-long effects on
674 soil properties, erosion, and ecosystem functioning (Foster et al. 2003, Cusack et al. 2013),
675 resulting in a large pool of NH_4^+ that can be recycled between the hypolimnion and sediments for
676 many years before eventual export (Ahlgren et al. 1994, Gerling et al. 2016).

677 Following expectation, hypolimnetic NO_3^- concentrations were significantly higher in
678 oxic conditions than anoxic conditions. Despite an increase in NO_3^- during oxic conditions, the
679 dominance of NH_4^+ over NO_3^- in the DIN pool (due to high NH_4^+ sediment fluxes even in oxic
680 conditions; Fig. 7) resulted in overall similar patterns for TN and NH_4^+ (Fig. 5C,D,E). We
681 initially anticipated that an increase in NO_3^- in oxic conditions could balance an increase in NH_4^+
682 in anoxic conditions, thereby resulting in similar DIN concentrations regardless of oxygen level,

683 but low nitrification rates prevented increases in NO_3^- from occurring in oxic conditions (Fig. 7,
684 Fig. S5). Long-term water chemistry monitoring of FCR shows much lower summer NO_3^-
685 concentrations over time relative to NH_4^+ (Fig. 3E,F), and thus modeled results follow
686 observations. In the anoxic scenario, denitrification rates at the sediments were higher than in the
687 water column, whereas in the oxic scenario, denitrification rates in the water column were higher
688 than at the sediments (Fig. 7, Fig. S5), as also observed in Swiss lakes with varying oxygen
689 levels (Müller et al. 2021).

690 Altogether, anoxia significantly decreased FCR's role as a NH_4^+ sink and simultaneously
691 increased its role as an NO_3^- sink (Fig. 8E,F), to the extent that ~100% of inflowing NO_3^- was
692 removed via denitrification. A previous study reported an average TN retention rate of 26% (and
693 up to 78%) of inputs for agricultural reservoirs in the U.S. (Powers et al. 2015). It would be
694 expected that FCR, which is located in a forested catchment, would have much higher TN
695 retention than agricultural reservoirs because of its lower external TN loads, however, FCR's
696 high export of NH_4^+ resulted in the reservoir serving as a source of TN downstream regardless of
697 hypolimnetic oxygen availability (Fig. 9). We anticipate that a greater duration and prevalence of
698 hypolimnetic anoxia in lakes and reservoirs could increase freshwater NO_3^- retention, while
699 decreasing TN retention if a waterbody's DIN pool is dominated by NH_4^+ , as in FCR.

700 Summer hypolimnetic DRP concentrations were approximately 3× higher in anoxic
701 conditions than oxic conditions (Fig. 5H). DRP cycling was primarily controlled by sediment
702 fluxes (Fig. 7), which encompassed both release from metal complexes and sediment organic
703 matter into the water column. Our observation of 2.2× higher sediment release rates of DRP in
704 anoxic than oxic conditions (Fig. 7) follows decades of work that have observed similar patterns

705 of increased P fluxes during anoxia (Mortimer 1971, Nürnberg 1987, Boström et al. 1988, Rydin
706 2000, Søndergaard et al. 2003).

707 A novel component of our study is that we simultaneously quantified both dissolved and
708 total pools of P at the whole-ecosystem scale in our model simulations, allowing us to
709 disentangle the responses of different P fractions to anoxia. While DRP concentrations tripled in
710 response to anoxia, TP concentrations only increased by 1.6× (Fig. 5G,H), indicating a lower
711 sensitivity of particulate P than DRP to hypolimnetic oxygen conditions in FCR. This result is
712 supported by the negligible (albeit statistically significant) response of POP to changes in oxygen
713 availability (Supplementary Text 5, Table S6). Consequently, we expect that the effects of
714 anoxia on reservoir TP dynamics are dependent on the proportion of dissolved P vs. particulate P
715 within the TP pool. If the hypolimnetic DRP pool comprises a sizeable proportion of TP, as
716 observed in FCR (median of 11±1%), then TP retention will likely be sensitive to anoxia (e.g.,
717 Fig. 9), but if DRP is lower, then TP cycling may be more resilient to anoxia.

718

719 *Shifts in stoichiometry in response to anoxia*

720 The substantial difference in stoichiometric ratios between anoxic and oxic conditions
721 has important implications for understanding how anoxia affects the ecosystem functioning of
722 lakes and reservoirs. Because anoxia increased hypolimnetic NH_4^+ concentrations more than any
723 other dissolved or total fraction in this study, and NH_4^+ dominated both the dissolved and total N
724 pools, any stoichiometric ratios that included NH_4^+ , DIN, or TN exhibited large shifts during
725 anoxia (Fig. 6). The significantly higher TN:TP and DIN:DRP ratios observed during anoxia will
726 likely affect water quality and food web structure (Fig. 6G,H). Higher N:P ratios favor non-N-
727 fixing cyanobacteria and will shift the composition of other taxa in phytoplankton community

728 based on their N and P requirements (Reynolds 2006), as phytoplankton can access hypolimnetic
729 nutrients via multiple mechanisms (Cottingham et al. 2015). In contrast, the significantly lower
730 TOC:TN, TOC:TP, DOC:DIN, DOC:NH₄⁺, and DOC:DRP ratios during anoxia (Fig.
731 6A,B,C,D,F) could increase organic matter mineralization rates (e.g., Coble et al. 2015).

732 Our results both support and contradict earlier studies that measured freshwater
733 stoichiometry across many waterbodies. Similar to an analysis of >27,000 freshwater samples
734 from U.S. waterbodies (Helton et al. 2015), we observed inverse relationships between NO₃⁻ vs.
735 NH₄⁺ concentrations and DOC vs. DIN concentrations (Fig. 6). Our study provides experimental
736 evidence to support the hypothesis that redox gradients are a major driver of NO₃⁻:NH₄⁺ and
737 DOC:DIN ratios, which will increase in oxic conditions and decrease in anoxic conditions
738 (Helton et al. 2015). On the other hand, our work finds only partial support for earlier findings of
739 lower TOC:TP and TN:TP ratios in reservoirs than natural lakes in an analysis of ~1000 U.S.
740 waterbodies, which was attributed in part to a greater incidence of anoxia in reservoirs
741 (Maranger et al. 2018). Median TOC:TP and TN:TP ratios in the reservoirs of that study were
742 417 and 38, respectively, which are similar to the ratios observed in FCR (Fig. 6B,G). While
743 anoxia decreased TOC:TP ratios (Fig. 6B), it also increased TN:TP ratios (Fig. 6G), suggesting
744 that anoxia is not responsible for all differences in stoichiometry between reservoirs and natural
745 lakes. Our results indicate that individual waterbodies' responses to anoxia may be dependent on
746 the dominance of NO₃⁻ vs. NH₄⁺ in their DIN pool prior to the onset of anoxia: if NO₃⁻
747 dominates, then TN:TP ratios will likely decrease with anoxia, while if NH₄⁺ dominates, then
748 TN:TP ratios will likely increase. In general, most lakes tend to have higher NO₃⁻ than NH₄⁺
749 concentrations (Quirós 2003, Leoni et al. 2018), suggesting that anoxia may result in lower
750 TN:TP ratios in most waterbodies.

751 *Opportunities and challenges of our whole-ecosystem approach*

752 Our coupled field manipulation and modeling study provided a powerful approach for
753 quantifying freshwater ecosystem responses to anoxia. By focusing on the same reservoir
754 experiencing different oxygen conditions over multiple years, we were able to isolate the effects
755 of oxygen on C, N, and P cycling without having to disentangle ecosystem-specific responses
756 (e.g., if we were comparing across multiple waterbodies). Ideally, we would have run the
757 REDOX field manipulation with multiple summers of continuous oxygenation and multiple
758 summers of no oxygenation to contrast hypolimnetic conditions. However, we were constrained
759 in our manipulation as the reservoir was an active drinking water source during the study,
760 necessitating us to activate the oxygenation system every summer for the preservation of water
761 quality. Consequently, we used the calibrated ecosystem model to simulate the biogeochemistry
762 of continuously oxygenated and never-oxygenated scenarios, which uniquely enabled us to
763 compare the effect of oxygenation while holding all other factors constant, such as temperature
764 (Fig. 4A). The similar biogeochemical responses to anoxia between the non-oxygenated vs.
765 oxygenated field data and the anoxic vs. oxic model scenarios support our integrated study
766 approach and the robustness of our findings (e.g., Fig. 5, Fig. S2).

767 The simulation model provided insights to reservoir responses to anoxia that would have
768 been challenging to glean from field observations alone. We used the model to calculate whole-
769 ecosystem rates that are impossible to measure in the field (e.g., daily POC burial), determine the
770 relative importance of different processes for biogeochemical budgets, and quantify how
771 processes changed in anoxic vs. oxic conditions. While the model's biogeochemical rates were
772 determined from automated optimization and calibration of numerical simulation parameters,
773 they fall within reasonable ranges of biogeochemical rates observed in the field, supporting our

774 model results. For example, hypolimnetic sediment flux chamber measurements that were
775 collected in FCR in summer 2018 measured a mean sediment oxygen demand of $\sim 20 \text{ mmol m}^{-2}$
776 d^{-1} (range $8\text{-}37.5 \text{ mmol m}^{-2} \text{ d}^{-1}$), which compares well with our calibrated hypolimnetic flux of
777 $29 \text{ mmol m}^{-2} \text{ d}^{-1}$ (Krueger et al. 2020). That study also measured NH_4^+ , DRP, and DOC fluxes
778 from the sediment into the water column as the chambers became anoxic, with calculated release
779 rates up to $2.7 \text{ mmol NH}_4^+ \text{ m}^{-2} \text{ d}^{-1}$, $0.01 \text{ mmol DRP m}^{-2} \text{ d}^{-1}$, and $14 \text{ mmol DOC m}^{-2} \text{ d}^{-1}$
780 (Supplementary Text 1). These numbers are consistent with our maximum calibrated rates of 2.8
781 $\text{mmol NH}_4^+ \text{ m}^{-2} \text{ d}^{-1}$ and $0.02 \text{ mmol DRP m}^{-2} \text{ d}^{-1}$ (Carey et al. 2021c). Our maximum calibrated
782 rate for DOC sediment flux, $1.4 \text{ mmol DOC m}^{-2} \text{ d}^{-1}$, is an order of magnitude lower than the field
783 data, suggesting that our modeled sediment flux rate of DOC was likely conservative.

784 We note several limitations to our study that should be considered. First, we focused on
785 the hypolimnion of FCR as a reactor in which we could isolate coupled biogeochemical
786 processes occurring during summer stratification, when C, N, and P processing rates are usually
787 at their highest due to warm temperatures. This focus on the hypolimnion precluded the analysis
788 of other important processes that can have large effects on biogeochemical cycling in the
789 epilimnion (e.g., photodegradation). Second, FCR has a hypolimnetic withdrawal, which results
790 in increased downstream export of hypolimnetic water from the reservoir. While export of
791 hypolimnetic water is limited in many naturally formed lakes, hypolimnetic withdrawals are very
792 common in reservoirs that provide drinking water, hydropower, and flood risk protection (Hayes
793 et al. 2017), which represent a large proportion of the reservoirs in the U.S. (NID 2021). Third,
794 the ecosystem model is inherently limited in that it does not include all processes that can affect
795 C, N, and P cycling (e.g., microbial dynamics, bioturbation). Fourth, similar to many other lake
796 modeling studies (e.g., Kara et al. 2012, Farrell et al. 2020, Ward et al. 2020), it was challenging

797 to model NO_3^- and DRP. For these solutes in particular, most of the variation in observations
798 was within the limit of quantitation (Supplementary Text 2), indicating that the model should not
799 necessarily be penalized for the low performance in its evaluation metrics. Despite these
800 challenges, the N and P parameters used for modeling FCR are consistent with other applications
801 of the GLM-AED for other lakes (e.g., Kara et al. 2012, Farrell et al. 2020, Ward et al. 2020),
802 and overall, we were generally able to recreate observed physical, chemical, and biological
803 dynamics in both the epilimnion and hypolimnion (Fig. 3, Figs. S3,S4). Moreover, the similarity
804 in results between the anoxic vs. oxic model scenarios and the field data from contrasting non-
805 oxygenated vs. oxygenated summer days (Fig. 5, Fig. S2) supports our approach and overall
806 results.

807

808 *Conclusions*

809 The duration, prevalence, and magnitude of anoxia in the bottom waters of lakes and
810 reservoirs are increasing globally (Butcher et al. 2015, Jenny et al. 2016a, Jane et al. 2021).
811 While low oxygen conditions are typically thought of as a response to land use and climate
812 change (Jenny et al. 2016b, Jane et al. 2021), our analysis demonstrates that low oxygen can also
813 be a *driver* of major changes to freshwater biogeochemical cycling.

814 Importantly, our work indicates that anoxia may alter the ability of freshwater ecosystems
815 to serve as sinks of C, N, and P in the landscape. Consequently, while hypolimnetic anoxia is a
816 result of increased C, N, and P loading into a waterbody, we also show that it may serve as an
817 intensifying feedback that increases anoxia in downstream waterbodies. This is evident in our
818 study, as we found significantly higher fluxes of C, N, and P downstream when FCR was
819 exhibiting anoxic vs. oxic conditions during the summer. Anoxia thus has the potential to both

820 degrade the water quality of downstream waterbodies and necessitate greater treatment of water
821 extracted from the reservoir for drinking. While more data are needed to evaluate the
822 consequences of this feedback on downstream water quality, we hypothesize that it could be an
823 important process affecting water quality in some freshwater ecosystems. Given the vital role
824 that inland waters play in removing C, N, and P from downstream export (Harrison et al. 2009,
825 Powers et al. 2016, Maranger et al. 2018), an increased prevalence and duration of anoxia in
826 lakes and reservoirs will likely have major effects on global C, N, and P budgets as well as water
827 quality and ecosystem functioning.

828

829 **Acknowledgments**

830 We thank the Western Virginia Water Authority, especially Jamie Morris, for their long-
831 term partnership and support. We thank Paul Gantzer, John Little, Jonathan Doubek, Kathryn
832 Krueger, Zackary Munger, and François Birgand for assistance with REDOX, and many field
833 and lab assistants past and present in the Reservoir Group. This work benefitted from discussions
834 with Nelson Hairston, Jr., Emil Rydin, and Kathleen Weathers and constructive feedback from
835 three reviewers. This study was financially supported by the National Science Foundation (DEB-
836 1753639, DEB-1753657, CNS-1737424, DBI-1933016, DGE-1651272), Fralin Life Sciences
837 Institute, Institute for Critical Technology and Applied Science, and Virginia Tech Global
838 Change Center.

839

840 **References**

841 Ahlgren, I., T. Waara, K. Vrede, and F. Soerensson. 1994. Nitrogen budgets in relation to
842 microbial transformations in lakes. *Ambio* **23**:367-377.

843 APHA. 2017. Standard Methods for the Examination of Water and Wastewater, 23rd Ed.
844 American Public Health Association, American Water Works Association, Washington
845 DC.

846 Bastviken, D., J. Cole, M. Pace, and L. Tranvik. 2004. Methane emissions from lakes:
847 Dependence of lake characteristics, two regional assessments, and a global estimate.
848 *Global Biogeochemical Cycles* **18**:GB4009.

849 Beaulieu, J. J., R. L. Smolenski, C. T. Nietch, A. Townsend-Small, M. S. Elovitz, and J. P.
850 Schubauer-Berigan. 2014. Denitrification alternates between a source and sink of nitrous
851 oxide in the hypolimnion of a thermally stratified reservoir. *Limnology and*
852 *Oceanography* **59**:495-506.

853 Beusen, A. H. W., A. F. Bouwman, L. P. H. Van Beek, J. M. Mogollón, and J. J. Middelburg.
854 2016. Global riverine N and P transport to ocean increased during the 20th century
855 despite increased retention along the aquatic continuum. *Biogeosciences* **13**:2441-2451.

856 Beutel, M., N. Burley, and K. Culmer. 2006. Quantifying the effects of water velocity and
857 oxygen on sediment oxygen demand. *Hydrological Sciences & Technology* **22**:271-228.

858 Beutel, M. W. 2003. Hypolimnetic anoxia and sediment oxygen demand in California drinking
859 water reservoirs. *Lake and Reservoir Management* **19**:208-221.

860 Boström, B., J. M. Andersen, S. Fleischer, and M. Jansson. 1988. Exchange of phosphorus
861 across the sediment-water interface. *Hydrobiologia* **170**:229-244.

862 Brett, M. T., S. K. Ahopelto, H. K. Brown, B. E. Brynstad, T. W. Butcher, E. E. Coba, C. A.
863 Curtis, J. T. Dara, K. B. Doeden, K. R. Evans, L. Fan, J. D. Finley, N. J. Garguilo, S. M.
864 Gebreyesus, M. K. Goodman, K. W. Gray, C. Grinnell, K. L. Gross, B. R. E. Hite, A. J.
865 Jones, P. T. Kenyon, A. M. Klock, R. E. Koshy, A. M. Lawler, M. Lu, L. Martinkosky, J.

866 R. Miller-Schulze, Q. T. N. Nguyen, E. R. Runde, J. M. Stultz, S. Wang, F. P. White, C.
867 H. Wilson, A. S. Wong, S. Y. Wu, P. G. Wurden, T. R. Young, and G. B. Arhonditsis
868 2016. The modeled and observed response of Lake Spokane hypolimnetic dissolved
869 oxygen concentrations to phosphorus inputs. *Lake and Reservoir Management* **32**:246-
870 258.

871 Brothers, S., J. Köhler, K. Attermeyer, H. P. Grossart, T. Mehner, N. Meyer, K. Scharnweber,
872 and S. Hilt. 2014. A feedback loop links brownification and anoxia in a temperate,
873 shallow lake. *Limnology and Oceanography* **59**:1388-1398.

874 Bruce, L., M. Frassl, G. Arhonditsis, G. Gal, D. Hamilton, P. Hanson, A. Hetherington, J.
875 Melack, J. Read, K. Rinke, A. Rigosi, D. Trolle, L. Winslow, R. Adrian, A. Ayala
876 Zamora, S. Bocaniov, B. Bohrer, C. Boon, J. Brookes, and M. Hipsey. 2018. A multi-
877 lake comparative analysis of the General Lake Model (GLM): Stress-testing across a
878 global observatory network. *Environmental Modelling and Software* **102**:274-291.

879 Butcher, J. B., D. Nover, T. E. Johnson, and C. M. Clark. 2015. Sensitivity of lake thermal and
880 mixing dynamics to climate change. *Climatic Change* **129**:295-305.

881 Carey, C. C., J. P. Doubek, R. P. McClure, and P. C. Hanson. 2018. Oxygen dynamics control
882 the burial of organic carbon in a eutrophic reservoir. *Limnology and Oceanography*
883 *Letters* **3**:293-301.

884 Carey, C. C., J. P. Doubek, J. H. Wynne, and B. R. Niederlehner. 2020. Dissolved silica time
885 series for Beaverdam Reservoir, Carvins Cove Reservoir, Claytor Lake, Falling Creek
886 Reservoir, Gatewood Reservoir, Smith Mountain Lake, and Spring Hollow Reservoir in
887 southwestern Virginia, USA during 2014, ver 1. Environmental Data Initiative
888 Repository. <https://doi.org/10.6073/pasta/353aa34bedfd68800c12275633811341>

889 Carey, C. C., A. G. Hounshell, M. E. Lofton, B. Birgand, B. J. Bookout, R. S. Corrigan, A. B.
890 Gerling, R. P. McClure, and W. M. Woelmer. 2021a. Discharge time series for the
891 primary inflow tributary entering Falling Creek Reservoir, Vinton, Virginia, USA 2013-
892 2021, ver 7. Environmental Data Initiative repository.
893 <https://doi.org/10.6073/pasta/8d22a432aac5560b0f45aa1b21ae4746>

894 Carey, C. C., A. S. Lewis, R. P. McClure, A. B. Gerling, S. Chen, A. Das, J. P. Doubek, D. W.
895 Howard, M. E. Lofton, K. D. Hamre, and H. L. Wander. 2021b. Time series of high-
896 frequency profiles of depth, temperature, dissolved oxygen, conductivity, specific
897 conductivity, chlorophyll a, turbidity, pH, oxidation-reduction potential, photosynthetic
898 active radiation, and descent rate for Beaverdam Reservoir, Carvins Cove Reservoir,
899 Falling Creek Reservoir, Gatewood Reservoir, and Spring Hollow Reservoir in
900 Southwestern Virginia, USA 2013-2020, ver 11. Environmental Data Initiative
901 repository. <https://doi.org/10.6073/pasta/5448f9d415fd09e0090a46b9d4020ccc>

902 Carey, C. C., R. Q. Thomas, and P. C. Hanson. 2021c. General Lake Model-Aquatic
903 EcoDynamics model parameter set for Falling Creek Reservoir, Vinton, Virginia, USA
904 2013-2019, ver 3. Environmental Data Initiative repository, [https://portal-](https://portal-s.edirepository.org/nis/mapbrowse?packageid=edi.471.3)
905 [s.edirepository.org/nis/mapbrowse?packageid=edi.471.3](https://portal-s.edirepository.org/nis/mapbrowse?packageid=edi.471.3).

906 Carey, C. C., R. Q. Thomas, R. P. McClure, A. G. Hounshell, W. M. Woelmer, H. L. Wander,
907 and A. S. L. Lewis. 2021d. CareyLabVT/FCR-GLM: FCR GLM-AED model, data, and
908 code for Carey et al. revised manuscript, v1.1. Zenodo,
909 <https://doi.org/10.5281/zenodo.6039335>

910 Carey, C. C., H. L. Wander, W. M. Woelmer, M. E. Lofton, A. Breef-Pilz, J. P. Doubek, A. B.
911 Gerling, A. G. Hounshell, R. P. McClure, and B. R. Niederlehner. 2021e. Water

912 chemistry time series for Beaverdam Reservoir, Carvins Cove Reservoir, Falling Creek
913 Reservoir, Gatewood Reservoir, and Spring Hollow Reservoir in southwestern Virginia,
914 USA 2013-2020, ver 8. Environmental Data Initiative repository.
915 <https://doi.org/10.6073/pasta/8d83ef7ec202eca9192e3da6dd34a4e0>

916 Carey, C. C., W. M. Woelmer, J. T. Maze, and A. G. Hounshell. 2019. Manually-collected
917 discharge data for multiple inflow tributaries entering Falling Creek Reservoir and
918 Beaverdam Reservoir, Vinton, Virginia, USA in 2019, ver 4. Environmental Data
919 Initiative repository. <https://doi.org/10.6073/pasta/4d8e7b7bedbc6507b307ba2d5f2cf9a2>

920 Carey, C. C., J. H. Wynne, H. L. Wander, R. P. McClure, K. J. Farrell, A. Breef-Pilz, J. P.
921 Doubek, A. B. Gerling, K. D. Hamre, A. G. Hounshell, A. S. Lewis, M. E. Lofton, and
922 W. M. Woelmer. 2021f. Secchi depth data and discrete depth profiles of
923 photosynthetically active radiation, temperature, dissolved oxygen, and pH for
924 Beaverdam Reservoir, Carvins Cove Reservoir, Falling Creek Reservoir, Gatewood
925 Reservoir, and Spring Hollow Reservoir in southwestern Virginia, USA 2013-2020, ver
926 8. Environmental Data Initiative repository.
927 <https://doi.org/10.6073/pasta/3e9f27971e353c8a80840b5e99a67d0c>

928 Coble, A., A. Marcarelli, and E. Kane. 2015. Ammonium and glucose amendments stimulate
929 dissolved organic matter mineralization in a Lake Superior tributary. *Journal of Great
930 Lakes Research* **41**:801-807.

931 Cole, J. J. 2013. *Freshwater Ecosystems and the Carbon Cycle*. Kinne, O., ed. *Excellence in
932 Ecology*, vol. 18. International Ecology Institute, Obendorf, Germany.

933 Cottingham, K. L., H. A. Ewing, M. L. Greer, C. C. Carey, and K. C. Weathers. 2015.
934 Cyanobacteria as biological drivers of lake nitrogen and phosphorus cycling. *Ecosphere*
935 **6**:art1. DOI: 10.1890/ES14-00174.1

936 Cusack, D. F., O. A. Chadwick, T. Ladefoged, and P. M. Vitousek. 2013. Long-term effects of
937 agriculture on soil carbon pools and carbon chemistry along a Hawaiian environmental
938 gradient. *Biogeochemistry* **112**:229-243.

939 Dillon, P. J., and L. A. Molot. 1997. Dissolved organic and inorganic carbon mass balances in
940 central Ontario lakes. *Biogeochemistry* **36**:29-42.

941 Downes, M. T. 1987. Aquatic nitrogen transformations at low oxygen concentrations. *Applied*
942 *and Environmental Microbiology* **54**:172-175.

943 Downing, J. A., Y. T. Prairie, J. J. Cole, C. M. Duarte, L. J. Tranvik, R. G. Striegl, W. H.
944 McDowell, P. Kortelainen, N. F. Caraco, J. M. Melack, and J. J. Middelburg. 2006. The
945 global abundance and size distribution of lakes, ponds, and impoundments. *Limnology*
946 *and Oceanography* **51**:2388-2397.

947 Farrell, K. J., N. K. Ward, A. I. Krinos, P. C. Hanson, V. Daneshmand, R. J. Figueiredo, and C.
948 C. Carey. 2020. Ecosystem-scale nutrient cycling responses to increasing air
949 temperatures vary with lake trophic state. *Ecological Modelling* **430**:109134.

950 Foster, D., F. Swanson, J. Aber, I. Burke, N. Brokaw, D. Tilman, and A. Knapp. 2003. The
951 importance of land-use legacies to ecology and conservation. *Bioscience* **53**:77-88.

952 Frindte, K., M. Allgaier, H.-P. Grossart, and W. Eckert. 2015. Microbial response to
953 experimentally controlled redox transitions at the sediment water interface. *PLoS One*
954 **10**:e0143428.

955 Gerling, A., R. Browne, P. Gantzer, M. Mobley, J. Little, and C. Carey. 2014. First report of the
956 successful operation of a side stream supersaturation hypolimnetic oxygenation system in
957 a eutrophic, shallow reservoir. *Water Research* **67**:129-143.

958 Gerling, A. B., Z. W. Munger, J. P. Doubek, K. D. Hamre, P. A. Gantzer, J. C. Little, and C. C.
959 Carey. 2016. Whole-catchment manipulations of internal and external loading reveal the
960 sensitivity of a century-old reservoir to hypoxia. *Ecosystems* **19**:555-571.

961 Hansen, N. 2016. The CMA evolution strategy: A tutorial. ArXiv **160400772**.
962 <https://arxiv.org/abs/1604.00772>

963 Hanson, P. C., M. L. Pace, S. R. Carpenter, J. J. Cole, and E. H. Stanley. 2015. Integrating
964 landscape carbon cycling: research needs for resolving organic carbon budgets of lakes.
965 *Ecosystems* **18**:363-375.

966 Harrison, J. A., R. J. Maranger, R. B. Alexander, A. E. Giblin, P.-A. Jacinthe, E. Mayorga, S. P.
967 Seitzinger, D. J. Sobota, and W. M. Wollheim. 2009. The regional and global
968 significance of nitrogen removal in lakes and reservoirs. *Biogeochemistry* **93**:143-157.

969 Hayes, N. M., B. R. Deemer, J. R. Corman, N. R. Razavi, and K. E. Strock. 2017. Key
970 differences between lakes and reservoirs modify climate signals: A case for a new
971 conceptual model. *Limnology and Oceanography-Letters* **2**:47-62.

972 Helton, A. M., M. Ardón, and E. S. Bernhardt. 2015. Thermodynamic constraints on the utility
973 of ecological stoichiometry for explaining global biogeochemical patterns. *Ecology*
974 *Letters* **18**:1049-1056.

975 Hipsey, M. R., L. C. Bruce, C. Boon, B. Busch, C. C. Carey, D. P. Hamilton, P. C. Hanson, J. S.
976 Read, E. de Sousa, M. Weber, and L. A. Winslow. 2019. A General Lake Model (GLM

977 3.0) for linking with high-frequency sensor data from the Global Lake Ecological
978 Observatory Network (GLEON). *Geoscience Model Development* **12**:473-523.

979 Hounshell, A. G., R. P. McClure, M. E. Lofton, and C. C. Carey. 2021. Whole-ecosystem
980 oxygenation experiments reveal substantially greater hypolimnetic methane
981 concentrations in reservoirs during anoxia. **6**:33-42.

982 Jane, S. F., G. J. A. Hansen, B. M. Kraemer, P. R. Leavitt, J. L. Mincer, R. L. North, R. M. Pilla,
983 J. T. Stetler, C. E. Williamson, R. I. Woolway, L. Arvola, S. Chandra, C. L. DeGasperi,
984 L. Diemer, J. Dunalska, O. Erina, G. Flaim, H.-P. Grossart, K. D. Hambright, C. Hein, J.
985 Hejzlar, L. L. Janus, J.-P. Jenny, J. R. Jones, L. B. Knoll, B. Leoni, E. Mackay, S.-I. S.
986 Matsuzaki, C. McBride, D. C. Müller-Navarra, A. M. Paterson, D. Pierson, M. Rogora, J.
987 A. Rusak, S. Sadro, E. Saulnier-Talbot, M. Schmid, R. Sommaruga, W. Thiery, P.
988 Verburg, K. C. Weathers, G. A. Weyhenmeyer, K. Yokota, and K. C. Rose. 2021.
989 Widespread deoxygenation of temperate lakes. *Nature* **594**:66-70.

990 Jenny, J.-P., P. Francus, A. Normandeau, F. Lapointe, M.-E. Perga, A. Ojala, A. Schimmelmann,
991 and B. Zolitschka. 2016a. Global spread of hypoxia in freshwater ecosystems during the
992 last three centuries is caused by rising local human pressure. *Global Change Biology*
993 **22**:1481-1489.

994 Jenny, J.-P., A. Normandeau, P. Francus, Z. E. Taranu, I. Gregory-Eaves, F. Lapointe, J. Jautzy,
995 A. E. K. Ojala, J.-M. Dorioz, A. Schimmelmann, and B. Zolitschka. 2016b. Urban point
996 sources of nutrients were the leading cause for the historical spread of hypoxia across
997 European lakes. *Proceedings of the National Academy of Sciences* **113**:12655.

998 Kara, E. L., P. Hanson, D. Hamilton, M. R. Hipsey, K. D. McMahon, J. S. Read, L. Winslow, J.
999 Dedrick, K. Rose, C. C. Carey, S. Bertilsson, D. da Motta Marques, L. Beversdorf, T.

1000 Miller, C. Wu, Y.-F. Hsieh, E. Gaiser, and T. Kratz. 2012. Time-scale dependence in
1001 numerical simulations: Assessment of physical, chemical, and biological predictions in a
1002 stratified lake at temporal scales of hours to months. *Environmental Modelling &*
1003 *Software* **35**:104-121.

1004 Kim, C., Y. Nishimura, and T. Nagata. 2006. Role of dissolved organic matter in hypolimnetic
1005 mineralization of carbon and nitrogen in a large, monomictic lake. *Limnology and*
1006 *Oceanography* **51**:70-78.

1007 Kortelainen, P., M. Rantakari, H. Pajunen, J. T. Huttunen, T. Mattsson, J. Alm, S. Juutinen, T.
1008 Larmola, J. Silvola, and P. J. Martikainen. 2013. Carbon evasion/accumulation ratio in
1009 boreal lakes is linked to nitrogen. *Global Biogeochemical Cycles* **27**:363-374.

1010 Krueger, K. M., C. E. Vavrus, M. E. Lofton, R. P. McClure, P. Gantzer, C. C. Carey, and M. E.
1011 Schreiber. 2020. Iron and manganese fluxes across the sediment-water interface in a
1012 drinking water reservoir. *Water Research* **182**:116003.

1013 Ladwig, R., P. C. Hanson, H. A. Dugan, C. C. Carey, Y. Zhang, L. Shu, C. J. Duffy, and K. M.
1014 Cobourn. 2021. Lake thermal structure drives interannual variability in summer anoxia
1015 dynamics in a eutrophic lake over 37 years. *Hydrology and Earth System Science*
1016 **25**:1009-1032.

1017 Lau, M. P., M. Sander, J. Gelbrecht, and M. Hupfer. 2016. Spatiotemporal redox dynamics in a
1018 freshwater lake sediment under alternating oxygen availabilities: combined analyses of
1019 dissolved and particulate electron acceptors. *Environmental Chemistry* **13**:826-837.

1020 Lehner, B., C. R. Liermann, C. Revenga, C. Vörösmarty, B. Fekete, P. Crouzet, P. Döll, M.
1021 Endejan, K. Frenken, J. Magome, C. Nilsson, J. C. Robertson, R. Rödel, N. Sindorf, and
1022 D. Wisser. 2011. High-resolution mapping of the world's reservoirs and dams for

1023 sustainable river-flow management. *Frontiers in Ecology and the Environment* **9**:494-
1024 502.

1025 Leoni, B., M. Patelli, V. Soler, and V. Nava. 2018. Ammonium transformation in 14 lakes along
1026 a trophic gradient. *Water* **10**. DOI: 10.3390/w10030265

1027 Maranger, R., S. E. Jones, and J. B. Cotner. 2018. Stoichiometry of carbon, nitrogen, and
1028 phosphorus through the freshwater pipe. *Limnology and Oceanography Letters* **3**:89-101.

1029 McDonald, C. P., E. G. Stets, R. G. Striegl, and D. Butman. 2013. Inorganic carbon loading as a
1030 primary driver of dissolved carbon dioxide concentrations in the lakes and reservoirs of
1031 the contiguous United States. *Global Biogeochemical Cycles* **27**:285-295.

1032 Mendonça, R., R. A. Müller, D. Clow, C. Verpoorter, P. Raymond, L. J. Tranvik, and S. Sobek.
1033 2017. Organic carbon burial in global lakes and reservoirs. *Nature Communications*
1034 **8**:1694.

1035 Medlyn, B. E., S. Zaehle, M. G. De Kauwe, A. P. Walker, M. C. Dietze, P. J. Hanson, T.
1036 Hickler, A. K. Jain, Y. Luo, W. Parton, I. C. Prentice, P. E. Thornton, S. Wang, Y.-P.
1037 Wang, E. Weng, C. M. Iversen, H. R. McCarthy, J. M. Warren, R. Oren, and R. J. Norby.
1038 2015. Using ecosystem experiments to improve vegetation models. *Nature Climate*
1039 *Change* **5**:528-534.

1040 Mendonça, R., R. A. Müller, D. Clow, C. Verpoorter, P. Raymond, L. J. Tranvik, and S. Sobek.
1041 2017. Organic carbon burial in global lakes and reservoirs. *Nature Communications*
1042 **8**:1694.

1043 Morris, M. D. 1991. Factorial sampling plans for preliminary computational experiments.
1044 *Technometrics* **33**:161-174.

1045 Mortimer, C. H. 1971. Chemical exchanges between sediments and water in the Great Lakes -
1046 speculations on probable regulatory mechanisms. *Limnology and Oceanography* **16**:387-
1047 404.

1048 Müller, B., R. Thoma, K. B. L. Baumann, C. M. Callbeck, and C. J. Schubert. 2021. Nitrogen
1049 removal processes in lakes of different trophic states from on-site measurements and
1050 historic data. *Aquatic Sciences* **83**:art37.

1051 Munger, Z. W., C. C. Carey, A. B. Gerling, J. P. Doubek, K. D. Hamre, R. P. McClure, and M.
1052 E. Schreiber. 2019. Oxygenation and hydrologic controls on iron and manganese mass
1053 budgets in a drinking-water reservoir. *Lake and Reservoir Management* **35**:277-291.

1054 NID 2021. U.S. National Inventory of Dams. Washington, DC: US Army Corps of Engineers.
1055 <https://nid.usace.army.mil/#/> Accessed on 2021-12-31.

1056 North, R. P., R. L. North, D. M. Livingstone, O. Köster, and R. Kipfer. 2014. Long-term changes
1057 in hypoxia and soluble reactive phosphorus in the hypolimnion of a large temperate lake:
1058 consequences of a climate regime shift. *Global Change Biology* **20**:811-823.

1059 Nürnberg, G. K. 1987. A comparison of internal phosphorus loads in lakes with anoxic
1060 hypolimnia. *Limnology and Oceanography* **32**:1160-1164.

1061 Nürnberg, G. K. 1988. Prediction of phosphorus release rates from total and reductant-soluble
1062 phosphorus in anoxic lake sediments. *Canadian Journal of Fisheries and Aquatic Sciences*
1063 **45**:453-462.

1064 Peter, S., O. Agstam, and S. Sobek. 2017. Widespread release of dissolved organic carbon from
1065 anoxic boreal lake sediments. *Inland Waters* **7**:151-163.

1066 Peter, S., A. Isidorova, and S. Sobek. 2016. Enhanced carbon loss from anoxic lake sediment
1067 through diffusion of dissolved organic carbon. *Journal of Geophysical Research:*
1068 *Biogeosciences* **121**:1959-1977.

1069 Powers, S. M., T. W. Bruulsema, T. P. Burt, N. I. Chan, J. J. Elser, P. M. Haygarth, N. J. K.
1070 Howden, H. P. Jarvie, Y. Lyu, H. M. Peterson, Andrew N. Sharpley, J. Shen, F. Worrall,
1071 and F. Zhang. 2016. Long-term accumulation and transport of anthropogenic phosphorus
1072 in three river basins. *Nature Geoscience* **9**:353-356.

1073 Powers, S. M., J. L. Tank, and D. M. Robertson. 2015. Control of nitrogen and phosphorus
1074 transport by reservoirs in agricultural landscapes. *Biogeochemistry* **124**:417-439.

1075 Quirós, R. 2003. The relationship between nitrate and ammonia concentrations in the pelagic
1076 zone of lakes. *Limnetica* **22**:37-50.

1077 Rydin, E. 2000. Potentially mobile phosphorus in Lake Erken sediment. *Water Research*
1078 **34**:2037-2042.

1079 Rysgaard, S., N. Risgaard-Petersen, N. Sloth, K. I. M. Jensen, and L. P. Nielsen. 1994. Oxygen
1080 regulation of nitrification and denitrification in sediments. *Limnology and Oceanography*
1081 **39**:1643-1652.

1082 Sharma, B., and R. C. Ahlert. 1977. Nitrification and nitrogen removal. *Water Research* **11**:897-
1083 925.

1084 Skoog, A. C., and V. A. Arias-Esquivel. 2009. The effect of induced anoxia and reoxygenation
1085 on benthic fluxes of organic carbon, phosphate, iron, and manganese. *Science of the*
1086 *Total Environment* **407**:6085-6092.

1087 Soares, L. M. V., and M. d. C. Calijuri. 2021. Deterministic modelling of freshwater lakes and
1088 reservoirs: Current trends and recent progress. *Environmental Modelling & Software*
1089 **144**:105143.

1090 Sobek, S., E. Durisch-Kaiser, R. Zurbrügg, N. Wongfun, M. Wessels, N. Pasche, and B. Wehrli.
1091 2009. Organic carbon burial efficiency in lake sediments controlled by oxygen exposure
1092 time and sediment source. *Limnology and Oceanography* **54**:2243-2254.

1093 Søndergaard, M., J. P. Jensen, and E. Jeppesen. 2003. Role of sediment and internal loading of
1094 phosphorus in shallow lakes. *Hydrobiologia* **506**:135-145.

1095 Sterner, R., and J. J. Elser. 2002. *Ecological Stoichiometry: The Biology of Elements From*
1096 *Molecules to The Biosphere*. Princeton University Press, Princeton, NJ.

1097 R Core Team. 2020. *R: A language and environment for statistical computing*. Version 3.6.3. R
1098 Foundation for Statistical Computing, Vienna, Austria.

1099 Toming, K., J. Kotta, E. Uemaa, S. Sobek, T. Kutser, and L. J. Tranvik. 2020. Predicting lake
1100 dissolved organic carbon at a global scale. *Scientific Reports* **10**:8471.

1101 Tranvik, L. J., J. A. Downing, J. B. Cotner, S. A. Loiselle, R. G. Striegl, T. J. Ballatore, P.
1102 Dillon, K. Finlay, K. Fortino, L. B. Knoll, P. L. Kortelainen, T. Kutser, S. Larsen, I.
1103 Laurion, D. M. Leech, S. L. McCallister, D. M. McKnight, J. M. Melack, E. Overholt, J.
1104 A. Porter, Y. Prairie, W. H. Renwick, F. Roland, B. S. Sherman, D. W. Schindler, S.
1105 Sobek, A. Tremblay, M. J. Vanni, A. M. Verschoor, E. von Wachenfeldt, and G. A.
1106 Weyhenmeyer. 2009. Lakes and reservoirs as regulators of carbon cycling and climate.
1107 *Limnology and Oceanography* **54**:2298-2314.

1108 Vachon, D., T. Langenegger, D. Donis, and D. F. McGinnis. 2019. Influence of water column
1109 stratification and mixing patterns on the fate of methane produced in deep sediments of a
1110 small eutrophic lake. *Limnology and Oceanography* **64**:2114–2128.

1111 Verpoorter, C., T. Kutser, D. A. Seekell, and L. J. Tranvik. 2014. A global inventory of lakes
1112 based on high-resolution satellite imagery. *Geophysical Research Letters* **41**:6396-6402.

1113 Walker, R. R., and W. J. Snodgrass. 1986. Model for sediment oxygen demand in lakes. *Journal*
1114 *of Environmental Engineering* **112**:25-43.

1115 Ward, N. K., B. G. Steele, K. C. Weathers, K. L. Cottingham, H. A. Ewing, P. C. Hanson, and C.
1116 C. Carey. 2020. Differential responses of maximum versus median chlorophyll-a to air
1117 temperature and nutrient loads in an oligotrophic lake over 31 years. *Water Resources*
1118 *Research* **56**:e2020WR027296.

1119 Wetzel, R. G. 2001. *Limnology: Lake and River Ecosystems*. 3rd edition. Academic Press, New
1120 York.

1121 Woolway, R. I., S. Sharma, G. A. Weyhenmeyer, A. Debolskiy, M. Golub, D. Mercado-Bettín,
1122 M. Perroud, V. Stepanenko, Z. Tan, L. Grant, R. Ladwig, J. Mesman, T. N. Moore, T.
1123 Shatwell, I. Vanderkelen, J. A. Austin, C. L. DeGasperi, M. Dokulil, S. La Fuente, E. B.
1124 Mackay, S. G. Schladow, S. Watanabe, R. Marcé, D. C. Pierson, W. Thiery, and E.
1125 Jennings. 2021. Phenological shifts in lake stratification under climate change. *Nature*
1126 *Communications* **12**:2318.

1127 Xia, Y., K. Mitchell, M. Ek, J. Sheffield, B. Cosgrove, E. Wood, L. Luo, C. Alonge, H. Wei, J.
1128 Meng, B. Livneh, D. Lettenmaier, V. Koren, Q. Duan, K. Mo, Y. Fan, and D. Mocko.
1129 2012. Continental-scale water and energy flux analysis and validation for the North
1130 American Land Data Assimilation System project phase 2 (NLDAS-2): 1.

- 1131 Intercomparison and application of model products. *Journal of Geophysical Research:*
1132 *Atmospheres* **117**:D03109.
- 1133 Zarfl, C., A. E. Lumsdon, J. Berlekamp, L. Tydecks, and K. Tockner. 2015. A global boom in
1134 hydropower dam construction. *Aquatic Sciences* **77**:161-170.
- 1135